GPR55 Signalling Promotes Proliferation of Pancreatic Cancer Cells and Tumour Growth in Mice, and its Inhibition Increases Effects of Gemcitabine

R Ferro,[1] A Adamska,[2] R Lattanzio,[3] I Mavrommati,[1] C E Edling,[1] S A Arifin,[1] C A Fyffe,[1] G Sala,[3] L Sacchetto,[4] G Chiorino,[4] V De Laurenzi,[2,3] M Piantelli,[3] O J Sansom,[5] T Maffucci[1] and M Falasca[*,1,2] .

[1]Queen Mary University of London, Barts and The London School of Medicine and Dentistry, Blizard Institute, Centre for Cell Biology and Cutaneous Research, 4 Newark Street, London E1 2AT, UK; [2]Metabolic Signalling Group, School of Biomedical Sciences, Curtin Health Innovation Research Institute, Curtin University, 6102 Perth, Western Australia; [3]Dipartimento di Scienze Mediche, Orali e Biotecnologiche, University "G. d'Annunzio" di Chieti-Pescara, Centro Studi sull'Invecchiamento, CeSI-MeT, Chieti 66100, Italy; [4]Cancer Genomics Laboratory, Fondazione Edo and Elvo Tempia, Biella, Italy; [5]Cancer Research UK Beatson Institute, Glasgow, G61 1BD, UK.

*Corresponding author:
Prof Marco Falasca
Metabolic Signalling Group, School of Biomedical Sciences, Curtin Health Innovation Research Institute, Curtin University, Perth, Western Australia 6102, Australia
Phone: +61 08 92669712
E-mail: marco.falasca@curtin.edu.au

Grant support: This work was supported by Pancreatic Cancer Research Fund and Avner Pancreatic Cancer Foundation (grants to MF). RF, CAF, CEE were supported by Pancreatic Cancer Research Fund (grants to MF). AA is supported by Curtin International Postgraduate Research Scholarship (CIPRS)/Health Sciences Faculty International Research Scholarship (HSFIRS). GS was supported by Ministero Sanità Finalizzata 2011/2012. VDL was supported by AIRC IG 15196.c.

Running title: Novel therapeutic options for PDAC

Abstract

The life expectancy for pancreatic cancer patients has seen no substantial changes in the last 40 years as very few and mostly just palliative treatments are available. As the five years survival rate remains around 5% the identification of novel pharmacological targets and development of new therapeutic strategies are urgently needed. Here we demonstrate that inhibition of the G protein-coupled receptor GPR55, using genetic and pharmacological approaches, reduces pancreatic cancer cell growth *in vitro* and *in vivo* and we propose that this may represent a novel strategy to inhibit pancreatic ductal adenocarcinoma (PDAC) progression. Specifically, we show that genetic ablation of *Gpr55* in the $KRAS^{WT/G12D}/TP53^{WT/R172H}/Pdx1\text{-}Cre^{+/+}$ (KPC) mouse model of PDAC significantly prolonged survival. Importantly, KPC mice treated with a combination of the GPR55 antagonist Cannabidiol (CBD) and gemcitabine (GEM, one of the most used drugs to treat PDAC), survived nearly three times longer compared to mice treated with vehicle or GEM alone. Mechanistically, knockdown or pharmacologic inhibition of GPR55 reduced anchorage dependent and independent growth, cell cycle progression, activation of mitogen-activated protein kinase (MAPK) signalling and protein levels of ribonucleotide reductases in PDAC cells. Consistent with this, genetic ablation of *Gpr55* reduced proliferation of tumour cells, MAPK signalling and ribonucleotide reductase M1 levels in KPC mice. Combination of CBD and GEM inhibited tumour cell proliferation in KPC mice and it opposed mechanisms involved in development of resistance to GEM *in vitro* and *in vivo*. Finally, we demonstrate that the tumour suppressor p53 regulates GPR55 protein expression through modulation of the microRNA miR34b-3p. Our results demonstrate the important role played by GPR55 downstream of p53 in PDAC progression. Moreover our data indicate that combination of CBD and GEM, both currently approved for medical use, might be tested in clinical trials as a novel promising treatment to improve PDAC patients' outcome.

Keywords: Pancreatic cancer, GPR55, gemcitabine, lysophosphatidylinositol.

INTRODUCTION

The progression from normal duct epithelium to infiltrating pancreatic ductal adenocarcinoma (PDAC) involves development of a characteristic pattern of precursors named pancreatic intraepithelial neoplasias (PanIN), histologically classified into distinct stages (PanIN 1a, PanIN 1b, PanIN 2, and PanIN 3) which eventually develop into PDAC, further classified in five distinct stages.[1] The genetic alterations associated with this process have been extensively characterised and they involve activating mutations of oncogenes, inactivating mutations of tumour suppressors as well as increased copy numbers of receptors.[2] For instance it is now well established that activating mutations of the oncogene *KRas* occur early during PanINs development and are detected in 85-90% of PDAC tumours.[3] On the other hand inactivating mutations of the tumour suppressor *TP53* occur in 70% of the latest stages of PanIN progression.[4] Transgenic mouse models have shed much light into the role of these specific mutations during PDAC development. The $KRAS^{WT/G12D}$/Pdx1-$Cre^{+/+}$ (KC) model which expresses a constitutively active KRas selectively in the pancreas is able to reproduce the PanIN lineage with a 100% penetrance but only few mice actually develop PDAC.[5] On the contrary the transgenic $KRAS^{WT/G12D}$/$TP53^{WT/R172H}$/Pdx1-$Cre^{+/+}$ (KPC) mice which additionally bear the *TP53* inactivating mutation develop the full PanIN range and PDAC with pathology very similar to human PDAC.[6] Therefore these transgenic models point to a key role for activated KRas in the early stage of neoplasias/cancer development and a central role for loss/inactivation of p53 in driving progression from the final PanINs stages to full PDAC.

In the last years our understanding of the genetic causes of PDAC has greatly increased but sadly this has not resulted in significant improvement of treatment options for patients. Surgical resection can lead to long-term survival and provides effective palliation but it is only applicable to patients with stage I and II PDAC. Chemotherapy and radiation therapy following the resection reduce metastatic development but these treatments result in little improvement of patient survival. Until very recently, Gemcitabine (GEM) was the only FDA-approved treatment for primary PDAC, but in most cases it can only prolong survival by several weeks.[7] Some combinations of drugs have proven slightly more successful although they still

effectively increase patients' survival by merely 2-4 months compared to GEM treatment.[8, 9] Several clinical trials are ongoing but currently PDAC remains one of the most aggressive cancers with a one year survival rate of 19% and five years survival rate of 5%.[10] Identification of novel pharmacological targets and development of new therapeutic strategies are urgently needed.[11]

Here we investigated the therapeutic potential of targeting the G protein-coupled receptor GPR55 in PDAC. GPR55 was identified as the receptor for the phospholipid lysophosphatidylinositol (LPI).[12] Increasing evidence now suggests that GPR55 plays an important role in many cancer types.[11] Whether targeting the receptor could ultimately result in improvement of survival and whether this strategy could represent a genuine novel therapeutic approach remains to be determined. Indeed, no study so far has investigated whether inhibition of GPR55 could improve survival of transgenic models that closely mirror the human disease.

Using genetic and pharmacological approaches we demonstrate that GPR55 has a central role in PDAC progression driven by *TP53* mutations. Furthermore, we show that inhibition of this receptor, especially in combination with GEM, reduces cancer progression and significantly improves survival in a transgenic mouse model of PDAC. These data provide the first evidence that inhibition of GPR55 represents a novel therapeutic strategy which can counteract PDAC progression and improve survival rate.

RESULTS

Genetic disruption of *Gpr55* inhibits pancreatic cancer proliferation *in vivo* and it improves survival in a PDAC mouse model

Immunohistochemistry (IHC) analysis of human normal pancreatic and PDAC specimens showed that GPR55 immunoreactivity was confined to the islets of Langerhans (Figure 1a) in normal pancreatic tissues, as previously reported,[13] while acinar cells and ducts were consistently negative (Figure 1a). On the other hand, GPR55 was expressed in 14 out of 54 human PDAC specimens (25.9%), indicating an accumulation of GPR55 in cancer tissues. Consistently, GPR55 was detected in PDAC specimens derived from implantation of patient-derived pancreatic cancer cells (patient-derived xenografts, PDX, Figure 1a) and in a panel of PDAC cell lines (Supplementary Figure 1a).

To determine the role of GPR55 in PDAC, KPC mice were crossed with mice harbouring homozygous deletion of *Gpr55* ($GPR55^{-/-}$)[14] to obtain the "KPCG" strain. Consistent with results from human tissues, IHC analysis indicated that GPR55 was specifically expressed by cells of the islets of Langerhans in Pdx1-$Cre^{+/+}$ and KPC mice, but not in KPCG mice (Supplementary Figure 1b). Moreover, expression of GPR55 was detected in PDAC cells from KPC but not KPCG mice (Supplementary Figure 1b), confirming the specificity of the anti-GPR55 antibody. Strikingly, genetic disruption of *Gpr55* significantly improved survival (Figure 1b). Specifically, the median survival was 32.5 days longer in KPCG mice (*n*=18) than in KPC mice (*n*=21). IHC analysis of corresponding dissected tumours indicated that GPR55 disruption reduced expression of the proliferative index Ki67 in the epithelial cells, specifically during the PanIN 2 and PanIN 3 progression stages (Figure 1c), indicating a role for GPR55 in pancreatic cancer cell proliferation.

These data demonstrate that GPR55 is crucial for PDAC development and/or progression *in vivo*.

GPR55 regulates cell cycle progression and MAPK signalling pathway.

Consistent with the *in vivo* data, siRNAs-mediated downregulation of GPR55 in PDAC cell lines significantly reduced cell proliferation (Supplementary Figures 2a and c and e) and anchorage-independent growth (Figures 2a and b). Efficient downregulation of GPR55 was confirmed by RT-qPCR (Supplementary Figures 2b and d and f). The inhibition of cell growth was mainly due to an effect on cell cycle progression as GPR55 downregulation significantly blocked the cell cycle at the G1/S transition phase (Supplementary Figures 3a and b) and reduced the mRNA levels of cyclins involved in regulation of the G1/S transition phase (including cyclin D1 and cyclin D2) without affecting mRNA levels of cyclin B1, which is involved in the G2/M transition (Supplementary Figure 3c). No increase in apoptosis was detected in PDAC cells upon GPR55 downregulation as assessed by Caspase 3 activity (Supplementary Figure 3d) or Annexin V/FACS (Supplementary Figure 3e) assays. These data demonstrate that GPR55 plays a specific role in PDAC cell proliferation/growth.

To further investigate the mechanism involved in cell growth and cell cycle regulation, the signalling pathways downstream of GPR55 were investigated in PDAC cells. As shown in Supplementary Figure 3f, phosphorylation of ERK1/2 at residues Threonine 202 and Tyrosine 204 was reduced in HPAFII cells transiently transfected with specific siRNAs targeting GPR55 compared to cells transfected with a non-targeting siRNA ("siControl") or incubated with transfection reagent alone ("untreated"). GPR55 downregulation further inhibited phosphorylation of S6 at its residues Serine 235/236 (Supplementary Figure 3f), which can be regulated downstream of the MAPK/ERK signalling pathway.[15] Efficient downregulation of GPR55 was confirmed by Western blot (Supplementary Figure 3f). No effect on the total levels of ERK and S6 was detected upon downregulation of GPR55 (Supplementary Figure 3f). Consistently, IHC analysis revealed a decrease in both ERK1/2 and S6 phosphorylation in tumour specimens from KPCG mice compared to KPC mice (Figure 2c and d).

These data indicate that one of the mechanisms by which GPR55 controls pancreatic cancer cell growth may be through regulation of the MAPK/ERK signalling pathway.

p53 regulates GPR55 protein expression through modulation of miR34b-3p levels.

To assess further the specific role of GPR55 during PDAC development/progression we crossed GPR55$^{-/-}$ mice with KC mice, which do not harbor the *TP53* mutation. No statistical differences were found in the survival of KC (*n*=19) compared to Gpr55$^{-/-}$/KRAS$^{WT/G12D}$/Pdx1-Cre$^{+/+}$ (KCG, *n*=12) mice, suggesting a role for the tumour suppressor p53 in the regulation of GPR55. To investigate this hypothesis, GPR55 protein expression was analysed in murine PDAC cell lines established from different transgenic mouse models. Results in Supplementary Figure 4a suggest that GPR55 protein expression is negatively associated with TP53 status, as the protein appears to be less expressed in the presence of wild type TP53 (PZR1 cells, derived from the KC model), whereas it is more expressed when TP53 is mutated (PZPR1 cells, derived from the KPC model) or deleted (PZPflR cells). Furthermore, overexpression of wild type p53 in ASPC1 cells (that harbour a *TP53* mutation) reduced the expression levels of GPR55 compared to cells transfected with the empty vector (Supplementary Figure 4b). On the other hand downregulation of p53 with two specific siRNAs strongly increased the expression levels of GPR55 in pancreatic cancer cells SW1990 that express wild type p53 (Figure 3b) and in HEK293T cells (Supplementary Figure 4c). These data indicate that wild type p53 negatively regulates GPR55 protein levels.

To gain further insight into the mechanisms of the p53-dependent regulation of GPR55, we performed luciferase assays using a plasmid containing the luciferase gene under the control of the 3'-untranslated region (3'-UTR) of *GPR55* ("GPR55" in Figure 3c). A plasmid encoding the luciferase gene but lacking a regulatory region was used as a control ("Control" in Figure 3c). ASPC1 cells were co-transfected with each luciferase plasmid in combination with either an empty vector (pcDNA) or plasmids encoding wild type p53 or mutants p53 (harboring mutations at positions 143^{Ala} or 175^{His}). Wild type and p53 mutants were expressed to similar levels in these experimental conditions (Supplementary Figure 4d). Results showed that the luciferase activity driven by 3'-UTR GPR55 was significantly decreased in cells expressing wild type p53 but not in cells expressing the mutant p53 (Figure 3c). These data demonstrate that wild type p53, but not its mutated forms, negatively affects GPR55 protein

expression by specifically regulating its 3'-UTR and influencing GPR55 mRNA degradation or translation. We next investigated whether the p53-dependent regulation of 3'-UTR GPR55 occurred directly or indirectly, possibly through regulation of microRNAs (miRs). More than one algorithm predicted GPR55 as a target of several miRs belonging to the miR34 family (Supplementary Table 1), which is known to be regulated by p53,[16] to be downregulated in PDAC and to have a key role in PDAC progression.[17] Specifically, we observed that miR34b-3p was the only miR within this family with a binding site on 3'-UTR GPR55 as predicted by MicroCosm (Supplementary Figure 4e), strongly suggesting that this specific miR could be involved in the p53-mediated regulation of GPR55 in PDAC cells. Consistent with this, we observed that miR34b-3p was downregulated in ASPC1 and HPAFII cells compared to the immortalised pancreatic cell line HPDE (Supplementary Figure 4f). Re-introduction of wild type p53 in ASPC1 cells increased miR34b-3p levels (Supplementary Figure 4g) while re-introduction of miR34b-3p in HPAFII and ASPC1 cells decreased GPR55 protein expression (Figure 3d).

These data indicate that wild type p53 downregulates GPR55 protein expression by modulating the levels of miR34b-3p (Figure 3e) and suggest a mechanism by which *TP53* mutations might promote cell growth through impaired regulation of miR34b-3p levels, which in turn results in increased expression of GPR55 and amplification of proliferative signals (Figure 3e).

Pharmacological inhibition of GPR55 reduces PDAC cell growth, cell cycle progression and MAPK signalling *in vitro*.

Our data so far demonstrated that pancreatic cancer cell proliferation *in vitro* and, importantly, PDAC progression *in vivo* could be inhibited by genetic *Gpr55* disruption. To validate the possibility of targeting GPR55 as a novel potential strategy in PDAC, we next investigated the effect of its pharmacological inhibition *in vitro* and *in vivo*. The GPR55 antagonist cannabidiol (CBD) efficiently inhibited anchorage-dependent growth of ASPC1, HPAFII, BXPC3 and PANC1 (Supplementary Figure 5a-d) cells. Similar results were obtained using the GPR55

antagonist CID16020046 (CID) in ASPC1 and HPAFII (Supplementary Figure 5a and b) cells. Treatment of HPAFII (Figure 4a) and PANC1 (Figure 4b) cells with CBD blocked cell cycle at the G1/S transition phase in a dose-dependent manner and it reduced DNA synthesis/entry in the S phase, as assessed by EdU incorporation (Figure 4c). Consistent with this, CBD reduced expression of cyclin D1 and activation of the tumour suppressor retinoblastoma (RB) without affecting the total levels of RB (Figure 4d). Inhibition of MEK/ERK and ERK-dependent pathways was also observed in cells treated with CBD (Figure 4e). On the other hand, no effect was detected on the total levels of any of the analysed proteins (Figure 4e). To investigate further the effect of CBD on different cell signalling pathways, we performed a human phospho-kinase array assay on lysates from untreated and CBD-treated HPAFII cells. Consistent with our previous data, results from the array confirmed a specific inhibition of ERK1/2 phosphorylation (25% threshold) upon treatment with CBD (Supplementary Figure 6). Importantly, Stat5a was the only other kinase whose phosphorylation appeared to be reduced by CBD treatment (25% threshold), although further investigation of additional, independent lysates did not confirm the Stat5a phosphorylation inhibition. Overall data from the array ruled out the possibility that CBD, at the concentrations used in this study, had many off target inhibitory effects on additional signalling pathways involved in regulation of cell growth and cell cycle progression. Finally, we observed that both CBD and CID inhibited anchorage-independent growth of ASPC1 and HPAFII cells (Figures 5a and b).

These data indicate that pharmacological inhibition of GPR55 reduces PDAC cell cycle progression and cell growth, suggesting that GPR55 may represent a novel target to counteract PDAC progression.

Pharmacological inhibition of GPR55 potentiates the effect of gemcitabine (GEM) *in vivo* and *in vitro*

We then investigated the effect of CBD on PDAC progression *in vivo* either alone or in combination with GEM. KPC mice were given CBD (100mg/kg), GEM (100mg/kg) or a combination of the two drugs, and survival curves were determined (Figure 5c). Lifespan

of mice given CBD (mean 25.4 days, median 22 days) was very similar to survival of mice given GEM (mean 27.8 days, median 23.5 days). Survival of mice given the vehicle was: mean 18.6 days, median 20 days. Strikingly, a remarkable and statistically significant increase in survival was observed when CBD was used in combination with GEM, with a nearly three-fold extension of mice survival compared to mice given the vehicle (mean 52.7 vs 18.6 days, median 56 vs 20 days). To determine the mechanism(s) underlying the pronounced effect of the drug combination on PDAC growth, we next analysed tumour specimens from the four groups of mice. IHC analysis indicated that combination of the two drugs strongly reduced the percentage of proliferative cells, as assessed by Ki67 staining (Figure 5d). Combination of CBD and GEM reduced the number of HPAFII (Supplementary Figure 7a) and PANC1 (Supplementary Figure 7b) cells more efficiently than each compound alone, as further confirmed by analysis of combination (CI) and dose reduction (DRI) indexes[18] using CompuSyn software (Supplementary Table 2).

These data indicate that combination of CBD and GEM strongly inhibits PDAC growth *in vitro* and *in vivo*.

Pharmacological inhibition of GPR55 affects signalling pathways involved in acquired resistance to GEM

IHC investigation revealed reduced ERK phosphorylation in tumours from mice given CBD (Figure 6a). A trend towards inhibition of S6 phosphorylation was also observed, although data did not reach statistical significance (Figure 6b). We detected increased ERK activation in tumours from mice given GEM compared to mice given the vehicle (Figure 6a). Increased ERK activation was previously reported upon GEM treatment and it was proposed as one of the mechanisms of acquired resistance to GEM treatment.[19] Importantly, IHC analysis of tumours from mice given a combination of CBD and GEM showed that CBD was able to counteract the effect of GEM on ERK and ultimately to reduce the GEM-dependent ERK phosphorylation (Figure 6a). Similarly, we observed that GEM increased ERK activation in HPAFII cells and this was opposed by CBD when the two drugs were used in combination

(Figure 6c). No effects were observed on ERK expression levels (Figure 6c). In the same experiments GEM induced phosphorylation of the histone variant H2AX (Figure 6c), a well-known marker of DNA damage.

Next, we investigated the effect of CBD on additional proposed mechanisms of GEM resistance. It was demonstrated that GEM can act by inhibiting the enzyme ribonucleotide reductase 1 (RRM1), leading to imbalance in the deoxyribonucleotides pool. Moreover, it was shown that cancer cell resistance can be associated with increased RRM1 and RRM2 expression.[20, 21] We observed that GPR55 downregulation reduced RRM1 protein expression in HPAFII cells (Figure 7a). Similarly, treatment with CBD reduced the levels of both RRM1 and RRM2 (Figure 7b). Moreover, reduced expression of RRM1 was detected in tumour specimens from KPCG compared to KPC mice (Figure 7c). Reduced levels of RRM1 mRNA were also observed in HPAFII cells upon treatment with CBD (Supplementary Figure 8a) and in KPCG compared to KPC mice (Supplementary Figure 8b). These data led us to hypothesise that CBD could counteract potential resistance mechanisms associated with upregulation of ribonucleotide reductases. Supporting this hypothesis, we detected increased expression of RRM1 in tumours from KPC mice given GEM (Figure 7d). While CBD alone did not seem to affect RRM1 levels, it was able to oppose the increase of RRM1 expression induced by GEM when the two drugs were used in combination (Figure 7d).

DISCUSSION

GPR55 has recently emerged as a key player in many cellular functions associated with cancer progression.[11] This role was initially suggested by the demonstration that GPR55 is the specific receptor for LPI[12, 22] whose role in cancer has been extensively described.[11, 23-25] From our original studies reporting the mitogenic properties of LPI[24, 26], data in literature have increasingly documented the involvement of LPI in several cellular processes required for cancer progression, including cancer cell proliferation, migration and angiogenesis.[22, 27, 28] Studies also demonstrated that Ras-transformed epithelial thyroid cells and fibroblasts[24, 26]

and different cancer cell lines[22, 28] are able to release LPI and increased levels of this phospholipid were found in ovarian cancer[29] and colon cancer[30] patients. Data indicating a specific requirement for GPR55 in modulation of most of the detected LPI-dependent functions provided the first indication that the receptor might be involved in cancer progression. Subsequent evidence supported this conclusion, including data demonstrating that GPR55 itself is overexpressed in many cancer cells[22, 27, 31, 32] and that GPR55 mRNA levels increase in human skin, larynx and oral squamous cell carcinoma compared to healthy tissues.[32] Increased levels of GPR55 mRNA were also detected in highly aggressive breast tumours[31] and high expression of GPR55 was recently associated with basal/triple-negative breast cancer subtype.[33]

A previous study reported increased levels of GPR55 mRNA in PanIN 2/3 compared to PanIN 1b.[31] GPR55 mRNA was also detected in the PDAC cell lines Mia PaCa-2[31] and PANC1,[34] the latter cells also expressing the receptor at the protein level.[34] Apart from these preliminary observations, no study has investigated whether accumulation of GPR55 occurs in PDAC and whether the receptor plays a role during PDAC development and progression. In this study, we show for the first time that GPR55 accumulates in human PDAC specimens compared to corresponding ductal areas in normal pancreatic tissue and it is detectable at the protein levels in a panel of PDAC cell lines. We demonstrate that the tumour suppressor p53 negatively regulates GPR55 protein expression in a mechanism involving regulation of miR34b-3p. As miR34b-3p itself was previously reported to be downregulated in PDAC and to have a key role in PDAC progression[35] our data identify a novel p53/miR34b-3p/GPR55 axis in this process.

We further show that downregulation and pharmacological inhibition of GPR55 reduced anchorage dependent and independent growth of PDAC cells, consistent with data previously indicating that GPR55 is an important regulator of cancer cell proliferation.[11, 22] More importantly we report that genetic disruption of *Gpr55* in KPC mice significantly reduced cancer cell proliferation *in vivo*, providing the first evidence that this receptor is important for pancreatic cancer proliferation in this established PDAC mouse model. Extensive *in vitro*

characterisation further demonstrated that growth inhibition was due to inhibition of cell cycle progression without increased apoptosis and it involved regulation of MAPK signalling pathways. Indication of a direct role of GPR55 in cancer progression was previously provided by the observation that GPR55$^{-/-}$ mice were more resistant to skin cancer development compared to wild type mice.[32] Similarly, delivery of siRNA targeting GPR55 in xenografts of T98G glioma cells reduced tumour growth *in vivo*.[31] Inhibition of metastasis formation was detected in mice injected with human colon cancer cells and treated with pharmacological inhibitors of GPR55[30] and in mice injected with human breast cancer cells lacking GPR55.[33] Adding to these data, our study provides the first demonstration that disruption of *Gpr55* can directly affect proliferation of the highly aggressive PDAC in the closest genetic model that is currently available to mimic the human disease and it can significantly extend the lifespan of KPC mice, providing the first evidence that targeting GPR55 can result in improvement of survival.

Although previous studies had provided preliminary indication that targeting GPR55 could potentially represent a novel therapeutic strategy in cancer[31, 32] no study so far had investigated whether pharmacological inhibition of GPR55 could directly improve survival in a model of PDAC. As we observed that GPR55 downregulation inhibited proliferation without inducing apoptosis, we decided to determine the effect of the GPR55 antagonist CBD alone or in combination with GEM, a cytotoxic drug currently used for PDAC treatment. It is worth mentioning that, although CBD has been confirmed to be a GPR55 antagonist, we could not completely rule out the possibility of additional effects of the drug, independent of GPR55 inhibition. However, the observation that similar data were obtained *in vitro* upon treatment with CBD or with the specific GPR55 antagonist CID as well as upon downregulation of GPR55 strongly supported the conclusion that the reduced cell growth/cell cycle progression detected in PDAC cells upon treatment with CBD was mainly due to inhibition of GPR55. Furthermore, results from the phospho-kinase array assay indicated that CBD did not inhibit activation of many signalling pathways, ruling out the possibility that the compound, at the concentrations used in our study, had many off target effects. Finally, we decided to use CBD in the *in vivo*

experiments as this drug is already approved for medical use therefore results from our study could have an immediate potential translational value. Here we report that KPC mice given a combination of CBD and GEM survived nearly three times longer compared to KPC mice given the vehicle (mean 52.7 vs 18.6 days, median 56 vs 20 days) and also longer than mice given GEM alone (mean 52.7 vs 27.8 days, median 56 vs 23.5). Our data further indicate that the remarkable increase in survival is likely due to the ability of the drugs combination to inhibit cancer cell proliferation and to overcome mechanisms involved in development of resistance to GEM treatment. To the best of our knowledge our study is the first demonstration that inhibition of GPR55 not only reduces cancer progression in a well-established transgenic model but it also represents a therapeutically valid strategy. In this respect, this study provides the first validation of GPR55 as a novel target for cancer treatment likely to be able to improve patients' outcome significantly.

The importance and clinical relevance of these results are further highlighted by the observation that they were obtained in a model of PDAC, one of the deadliest cancer types and in urgent need of novel treatment options. The very few therapeutic options currently available for advanced PDAC solely increase survival by few months leaving the five years survival rate at a mere 5%. Development of drug resistance is one of the main reasons for such an abysmal prognosis. Our demonstration that combination of CBD and GEM can oppose mechanisms associated with drug resistance and increase survival of KPC mice is very important considering that both drugs are already approved for medical use and therefore this combination can be quickly tested in clinical trials.

In conclusion, our study identified GPR55 as a novel critical mediator of PDAC development and progression. The demonstration that GPR55 is negatively regulated by p53 and it controls cell cycle progression and growth of pancreatic cancer cells provides novel information into the mechanisms by which *TP53* mutations can lead to PDAC development. Moreover, our study provides the first evidence that GPR55 is a therapeutically valid target whose inhibition, in particular in combination with GEM, results in improved survival in the transgenic model closest to the human disease currently available. These results represent a

huge step forward towards the identification of a novel treatment regime that could highly benefit PDAC patients.

MATERIALS AND METHODS

Mouse strains

All animal experiments were conducted in compliance with institutional and national guidelines. Mice were housed in ventilated cages under standardized conditions (21°C, 60% humidity, 12-hour light/12-hour dark cycle, 20 changes air/hour), palpated daily and culled by carbon dioxide-mediated asphyxiation or cervical dislocation. $KRAS^{WT/G12D}$/$TP53^{WT/R172H}$/Pdx1-$Cre^{+/+}$ (KPC), $KRAS^{WT/G12D}$/Pdx1-$Cre^{+/+}$ (KC) and Pdx1-$Cre^{+/+}$ mice were kindly provided by Prof. David A. Tuveson (Cancer Center at Cold Spring Harbor Laboratory). $GPR55^{-/-}$ mice were kindly provided by Prof. David Baker (Queen Mary University of London). $GPR55^{-/-}$ mice and KPC control mice were maintained on a GPR55 background. Mice were ear marked and specimen genotyped via DNA extraction and PCR (out sourced to Transnetyx Inc.). KPC mice used for drug treatments were maintained on a mixed C57BL/6,129Sv1 background. KPC mice were treated with CBD (GW Pharmaceuticals, 100mg/kg), GEM (100mg/kg), and with a combination of the two treatments. Mice enrolment was based on tumour size, measured by palpation. Specifically, mice underwent palpation every 24 h once they reached 80 days of age (predicted age when tumours should start to develop). Mice were assigned to the four arms (vehicle, CBD, GEM, CBD+GEM) by simple randomisation using a shuffled deck of cards as described.[36] Vehicle and CBD were administered by daily intraperitoneal injection while GEM was administered by intraperitoneal injection every three days. Mice were checked daily and left until death or culled when pre-assigned end points were reached. The pre-assigned end points included mice displaying one of the following: development of abdominal ascites, severe cachexia, significant weight loss (approaching 20% of initial weight), extreme weakness, inactivity, discomfort or pain. No major side/adverse effects and no weight loss were observed in mice treated with CBD.

Immunohistochemistry (IHC)

Mouse pancreatic tissues were placed in 10% neutral-buffered formalin immediately after sacrifice and incubated for at least 24 h. After embedding and sectioning procedures, tissues were stained with Hematoxylin and Eosin (H&E) to confirm the presence of tumours. Antibody staining was performed on 5 µm thick sections with the following antibodies and dilutions: GPR55 (1M urea buffer; dilution 1:100, 1:800; Novus Biologicals); $pERK^{T202/Y204}$ (pH 6.0; dilution 1:75; Cell Signaling Technology); $pS6^{S235/236}$ (pH 9.0; dilution 1:100; Cell Signaling Technology); RRM1 (pH 6.0; dilution 1:250; Abcam); Ki67 (pH 6.0; dilution 1:75; eBioscience). Representative images of antibody optimisation are shown in Supplementary Table 3. IHC slides were scored independently by two pathologists (RL and MP) blind to molecular data. The normal pancreatic tissue presented in Figure 1a was obtained from a patient without any findings of pancreatic cancer.

Tissue microarray (TMA)

Archived formalin-fixed, paraffin-embedded blocks from 54 patients diagnosed with primary PDAC were retrieved at the “Regina Elena” National Cancer Institute (Rome, Italy). TMA were constructed by removing 2-mm diameter cores of histologically confirmed tumor areas. TMA sections were then incubated with anti-GPR55 rabbit polyclonal antibody (dilution 1:100, incubation overnight, Novus Biologicals) after antigen retrieval by microwave treatment at 750 W for 10 min in 1M urea buffer. Anti-rabbit EnVision kit (K4003, Dako, Glostrup, Denmark) was used for signal amplification. In control sections, the primary antibody was replaced with isotype-matched immunoglobulins. The expression of markers was quantified as percent of immunoreactive cells.

Statistics

All sample sizes were chosen based prior studies performed in our laboratories and appropriate power calculations performed by expert biostatisticians of the School of Public Health at Curtin University. Unless otherwise specified Student's t-Test (one sided) was used to determine statistical significance. In each case: *$p<0.05$, **$p<0.01$, ***$p<0.001$, ****$p<0.0001$

Additional Materials and Methods are in Supplementary Information

CONFLICT OF INTEREST

The authors declare no conflict of interest.

ACKNOWLEDGEMENTS

This work was supported by Pancreatic Cancer Research Fund and Avner Pancreatic Cancer Foundation (grants to MF). RF, CAF, CEE were supported by Pancreatic Cancer Research Fund (grants to MF). AA is supported by Curtin International Postgraduate Research Scholarship (CIPRS)/Health Sciences Faculty International Research Scholarship (HSFIRS). GS was supported by Ministero Sanità Finalizzata 2011/2012. VDL was supported by AIRC IG 15196.c. We thank Prof David A.Tuveson and Prof David Baker for KC/KPC and GPR55$^{-/-}$ mice respectively; Dr Massimo Broggini for p53 mutants constructs; Prof Hemant Kocher for HPDE cells; GW Pharmaceuticals for providing the cannabidiol used in this study; the Pathology Core facility of the Blizard Institute for helping with IHC. AA, VDL and MF also acknowledge the infrastructure and staff support provided by CHIRI, School of Biomedical Sciences and Faculty of Health Sciences, Curtin University.

Author Contributions

RF and MF designed, coordinated, and carried out the bulk of the experiments. RF, AA, IM, TM, and MF performed *in vitro* experiments. RF, TM, and MF designed and supervised *in vitro* experiments. RF, GS, and MF designed and supervised *in vivo* experiments. RF performed *in vivo* experiments. SAA, CAF, CEE, and VDL contributed to *in vivo* experiments. RF and RL performed IHC assay. RL and MP performed IHC analysis. LS and GC performed in silico analysis. OJS. provided key reagents. RF, TM, and MF wrote the manuscript. MF conceived the project, led and supervised the study.

Supplementary Information accompanies the paper on the *Oncogene* website (http://www.nature.com/onc)

REFERENCES

1 Hruban RH, Goggins M, Parsons J, Kern SE. Progression model for pancreatic cancer. Clin Cancer Res 2000; 6: 2969-2972.

2 Hruban RH, Wilentz RE, Kern SE. Genetic progression in the pancreatic ducts. Am J Pathol 2000; 156: 1821-1825.

3 Eser S, Schnieke A, Schneider G, Saur D. Oncogenic KRAS signalling in pancreatic cancer. Br J Cancer 2014; 111: 817-822.

4 Scarpa A, Capelli P, Mukai K, Zamboni G, Oda T, Iacono C *et al*. Pancreatic adenocarcinomas frequently show p53 gene mutations. Am J Pathol 1993; 142: 1534-1543.

5 Hingorani SR, Petricoin EF, Maitra A, Rajapakse V, King C, Jacobetz MA *et al*. Preinvasive and invasive ductal pancreatic cancer and its early detection in the mouse. Cancer Cell 2003; 4: 437-450.

6 Hingorani SR, Wang L, Multani AS, Combs C, Deramaudt TB, Hruban RH *et al*. Trp53R172H and KrasG12D cooperate to promote chromosomal instability and widely metastatic pancreatic ductal adenocarcinoma in mice. Cancer Cell 2005; 7: 469-483.

7 Morris JP, Wang SC, Hebrok M. KRAS, Hedgehog, Wnt and the twisted developmental biology of pancreatic ductal adenocarcinoma. Nat Rev Cancer 2010; 10: 683-695.

8 Peixoto RD, Ho M, Renouf DJ, Lim HJ, Gill S, Ruan JY *et al*. Eligibility of Metastatic Pancreatic Cancer Patients for First-Line Palliative Intent nab-Paclitaxel Plus Gemcitabine Versus FOLFIRINOX. Am J Clin Oncol 2015.

9 Vaccaro V, Sperduti I, Milella M. FOLFIRINOX versus gemcitabine for metastatic pancreatic cancer. N Engl J Med 2011; 365: 768-769; author reply 769.

10 Vincent A, Herman J, Schulick R, Hruban RH, Goggins M. Pancreatic cancer. Lancet 2011; 378: 607-620.

11 Falasca M, Kim M, Casari I. Pancreatic cancer: Current research and future directions. Biochim Biophys Acta 2016; 1865: 123-132.

12 Oka S, Nakajima K, Yamashita A, Kishimoto S, Sugiura T. Identification of GPR55 as a lysophosphatidylinositol receptor. Biochem Biophys Res Commun 2007; 362: 928-934.

13 Romero-Zerbo SY, Rafacho A, Diaz-Arteaga A, Suarez J, Quesada I, Imbernon M *et al*. A role for the putative cannabinoid receptor GPR55 in the islets of Langerhans. J Endocrinol 2011; 211: 177-185.

14 Sisay S, Pryce G, Jackson SJ, Tanner C, Ross RA, Michael GJ *et al*. Genetic background can result in a marked or minimal effect of gene knockout (GPR55 and CB2 receptor) in experimental autoimmune encephalomyelitis models of multiple sclerosis. PLoS One 2013; 8: e76907.

15 Roux PP, Shahbazian D, Vu H, Holz MK, Cohen MS, Taunton J *et al*. RAS/ERK signaling promotes site-specific ribosomal protein S6 phosphorylation via RSK and stimulates cap-dependent translation. J Biol Chem 2007; 282: 14056-14064.

16 He L, He X, Lim LP, de Stanchina E, Xuan Z, Liang Y *et al*. A microRNA component of the p53 tumour suppressor network. Nature 2007; 447: 1130-1134.

17 Vogt M, Munding J, Gruner M, Liffers ST, Verdoodt B, Hauk J *et al*. Frequent concomitant inactivation of miR-34a and miR-34b/c by CpG methylation in colorectal, pancreatic, mammary, ovarian, urothelial, and renal cell carcinomas and soft tissue sarcomas. Virchows Arch 2011; 458: 313-322.

18 Chou TC. Theoretical basis, experimental design, and computerized simulation of synergism and antagonism in drug combination studies. Pharmacol Rev 2006; 58: 621-681.

19 Zheng C, Jiao X, Jiang Y, Sun S. ERK1/2 activity contributes to gemcitabine resistance in pancreatic cancer cells. J Int Med Res 2013; 41: 300-306.

20 Davidson JD, Ma L, Flagella M, Geeganage S, Gelbert LM, Slapak CA. An increase in the expression of ribonucleotide reductase large subunit 1 is associated with gemcitabine resistance in non-small cell lung cancer cell lines. Cancer Res 2004; 64: 3761-3766.

21 Bergman AM, Eijk PP, Ruiz van Haperen VW, Smid K, Veerman G, Hubeek I *et al*. In vivo induction of resistance to gemcitabine results in increased expression of ribonucleotide reductase subunit M1 as the major determinant. Cancer Res 2005; 65: 9510-9516.

22 Pineiro R, Maffucci T, Falasca M. The putative cannabinoid receptor GPR55 defines a novel autocrine loop in cancer cell proliferation. Oncogene 2011; 30: 142-152.

23 Ross RA. L-α-Lysophosphatidylinositol meets GPR55: a deadly relationship. Trends in Pharmacological Sciences 2011; 32: 265-269.

24 Falasca M, Corda D. Elevated levels and mitogenic activity of lysophosphatidylinositol in k-ras-transformed epithelial cells. Eur J Biochem 1994; 221: 383-389.

25 Falasca M, Iurisci C, Carvelli A, Sacchetti A, Corda D. Release of the mitogen lysophosphatidylinositol from H-Ras-transformed fibroblasts; a possible mechanism of autocrine control of cell proliferation. Oncogene 1998; 16: 2357-2365.

26 Falasca M, Silletta MG, Carvelli A, Di Francesco AL, Fusco A, Ramakrishna V *et al*. Signalling pathways involved in the mitogenic action of lysophosphatidylinositol. Oncogene 1995; 10: 2113-2124.

27 Ford LA, Roelofs AJ, Anavi-Goffer S, Mowat L, Simpson DG, Irving AJ *et al*. A role for L-alpha-lysophosphatidylinositol and GPR55 in the modulation of migration, orientation and polarization of human breast cancer cells. Br J Pharmacol 2010; 160: 762-771.

28 Hofmann NA, Yang J, Trauger SA, Nakayama H, Huang L, Strunk D *et al*. The GPR 55 agonist, L-alpha-lysophosphatidylinositol, mediates ovarian carcinoma cell-induced angiogenesis. Br J Pharmacol 2015; 172: 4107-4118.

29 Sutphen R, Xu Y, Wilbanks GD, Fiorica J, Grendys EC, Jr., LaPolla JP *et al*. Lysophospholipids are potential biomarkers of ovarian cancer. Cancer Epidemiol Biomarkers Prev 2004; 13: 1185-1191.

30 Kargl J, Andersen L, Hasenohrl C, Feuersinger D, Stancic A, Fauland A *et al*. GPR55 promotes migration and adhesion of colon cancer cells indicating a role in metastasis. Br J Pharmacol 2016; 173: 142-154.

31 Andradas C, Caffarel MM, Perez-Gomez E, Salazar M, Lorente M, Velasco G *et al*. The orphan G protein-coupled receptor GPR55 promotes cancer cell proliferation via ERK. Oncogene 2011; 30: 245-252.

32 Perez-Gomez E, Andradas C, Flores JM, Quintanilla M, Paramio JM, Guzman M *et al*. The orphan receptor GPR55 drives skin carcinogenesis and is upregulated in human squamous cell carcinomas. Oncogene 2013; 32: 2534-2542.

33 Andradas C, Blasco-Benito S, Castillo-Lluva S, Dillenburg-Pilla P, Diez-Alarcia R, Juanes-Garcia A *et al*. Activation of the orphan receptor GPR55 by lysophosphatidylinositol promotes metastasis in triple-negative breast cancer. Oncotarget 2016.

34 Paul RK, Wnorowski A, Gonzalez-Mariscal I, Nayak SK, Pajak K, Moaddel R *et al*. (R,R ')-4 '-methoxy-1-naphthylfenoterol targets GPR55-mediated ligand internalization and impairs cancer cell motility. Biochem Pharmacol 2014; 87: 547-561.

35 Ji Q, Hao XB, Zhang M, Tang WH, Meng Y, Li L *et al*. MicroRNA miR-34 Inhibits Human Pancreatic Cancer Tumor-Initiating Cells. Plos One 2009; 4.

Figure Legends

Figure 1. Genetic disruption of *Gpr55* reduces PDAC growth *in vivo*. (**a**) Representative images of GPR55 protein expression in human normal pancreas, PDAC, and PDX tissues assessed by IHC. Scale bar: 50µm. Blue dotted lines indicate Islet of Langerhans, red dotted line indicates normal pancreatic duct. (**b**) Kaplan-Meier survival curves of KPC (*n*=18) and KPCG (*n*=21) mice. Logrank (Mantel-Cox) test p=0.0013, Gehan-Breslow-Wilcoxon test p=0.0032. Representative H&E staining of tissues from KPC and KPCG mice confirms presence of PDAC. Scale bar: 250µm. (**c**) Representative images of Ki67 protein expression in tissues from KPC and KPCG at the indicated stages of PanIN progression. Scale bar: 50µm. Graphs indicate the percentage of PanIN cells showing Ki67 staining. *p<0.05.

Figure 2. *In vitro and in vivo* effects of GPR55 downregulation. (**a,b**) The indicated PDAC cell lines were transfected with a non-targeting siRNA (siControl) or siRNAs specifically targeting GPR55 and plated on soft agar as described in the Materials and Methods. Colonies were allowed to grow for 3-4 weeks. Data are means ± s.e.m. of n=3 independent experiments performed in duplicate. *p<0.05, **p<0.01 vs siControl. (**c,d**) Representative images of PDAC specimens from KPC and KPCG mice stained with antibodies recognising phosphorylated $ERK^{T202/Y204}$ (**c**) and $S6^{S235/236}$ (**d**). Scale bar: 50µm. Graphs indicate the percentage of PDAC cells showing positive staining for each antibody. *p<0.05.

Figure 3. p53 regulates GPR55 protein levels in PDAC. (**a**) Kaplan-Meier survival curves of KC (*n*=19) and KCG (*n*=12) mice. Log-rank (Mantel-Cox) test p=0.17198, Gehan-Breslow-Wilcoxon test p=0.9677. Representative images of H&E staining confirm presence of tumours. Scale bar: 250µm. (**b**) Pancreatic cancer cells SW1990, expressing wild type p53, were transfected with siRNAs targeting p53 or siControl and lysed after 48h. Representative Western blot and results from densitometry analysis are shown. Actinin was used as loading control. Data are means ± s.e.m. of *n*=3 independent experiments and are expressed as fold change of normalised GPR55 levels in cells transfected with siControl. *p<0.05. (**c**) Luciferase activity assays were performed in ASPC1 co-transfected with the indicated plasmids as specified in the Materials and Methods. Results are means ± s.e.m. of *n*=5 independent

experiments. *p<0.05. (**d**) The effect of re-introduction of miR34b-3p in ASPC1 and HPAFII cells on GPR55 protein expression was assessed by Western blot. Vinculin was used as loading control. Data from densitometry analysis are expressed as fold change of normalised GPR55 levels in cells transfected with miR control and are means ± s.e.m. of *n*=3 independent experiments. *p<0.05, **p<0.01. (**e**) Proposed model of p53/GPR55 signalling. Wild type, active p53 negatively regulates GPR55 protein expression by increasing miR34b-3p levels. The reduced GPR55 protein levels result in a weak proliferative signal. Mutated p53 is not able to regulate miR34b-3p levels and therefore GPR55 protein expression is not affected. High GPR55 protein expression results in a strong proliferative signal. Dotted arrows indicate inhibition; solid arrows indicate activation.

Figure 4. Pharmacological inhibition of GPR55 inhibits cell cycle progression and MAPK signalling pathways. HPAFII (**a**) and PANC1 (**b**) cells were treated for 72h with the indicated concentrations of CBD or vehicle alone ("untreated") in DMEM containing 10% FBS. Cell cycle analysis was performed by FACS. Results are expressed as percentage of cells in each phase of the cycle and are means ± s.e.m. of *n*=3 independent experiments. *p<0.05, **p<0.01. (**c**) HPAFII cells were treated with the indicated concentrations of CBD for 70h before incubation with 10μM EdU for further 2h. Graph indicates the percentage of cells that had incorporated EdU. Data are expressed as fold change of cells treated with vehicle ("untreated") and are means ± s.e.m. of *n*=3 independent experiments performed in duplicate. **p<0.01, ***p<0.001. (**d**) Effect of CBD treatment on the cell cycle regulators Cyclin D1 and pRB^{S795}. Total levels of RB were also assessed. Tubulin was used as loading control. (**e**) Effect of CBD treatment on activation and total levels of the indicated members of the MAPK/ERK signalling pathway. Tubulin or vinculin were used as loading controls. Results from densitometry analysis are expressed as fold change of normalised results from cells incubated with vehicle ("untreated") and are means ± s.e.m. of *n*=3 independent experiments apart from: $pERK^{T202/Y204}$ (*n*=7-9), $pS6^{S235/236}$ (*n*=6), pRB^{S795} and RB (*n*=4). *p<0.05, **p<0.01, ***p<0.001, ****p<0.0001.

Figure 5. Pharmacological inhibition of GPR55 inhibits anchorage-independent growth of PDAC cells and potentiates the effect of GEM *in vivo*. (**a,b**) Effect of CDB and CID on

anchorage-independent growth of ASPC1 (**a**) and HPAFII (**b**) cells. Colonies were allowed to grow for 3-4 weeks. Control cells were incubated with the corresponding amount of vehicle ("untreated"). Data are means ± s.e.m. of *n*=3 independent experiments performed in duplicate. *p<0.05, **p<0.01 vs control cells. (**c**) Kaplan-Meier survival curves of KPC mice given the vehicle (*n*=9), CBD (*n*=10), GEM (*n*=8), and CBD plus GEM (*n*=7). Curves indicate days after start of each treatment. Logrank (Mantel-Cox) test p=0.0059, Logrank test for trend p=0.0007, Gehan-Breslow-Wilcoxon test p=0.0268. Images show representative H&E staining confirming the presence of tumours. Scale bar: 250μm. (**d**) Representative images of Ki67 protein expression in PDAC specimens from each group of mice. Scale bar: 50μm. Graph indicates the percentage of PDAC cells showing Ki67 staining. *p<0.05.

Figure 6. Effect of drugs combination on MAPK signalling pathway *in vitro* and *in vivo*. (**a,b**) Representative images of PDAC specimens from KPC mice given the indicated drugs, stained with antibodies recognising $pERK^{T202/Y204}$ (**a**) and $pS6^{S235/236}$ (**b**). Scale bar: 50μm. Graphs indicate the percentage of PDAC cells showing positive staining for each antibody. *p<0.05. (**c**) HPAFII cells were incubated in DMEM containing 10% FBS supplemented with 10μM CBD or 20nM GEM alone or in combination for 48h. Phosphorylation of $ERK^{T202/Y204}$ and H2AX and levels of ERK were assessed by Western blotting analysis. Vinculin was used as loading control. Data from densitometry analysis are expressed as fold change of normalised results from cells incubated with vehicle ("untreated") and are means ± s.e.m. of *n*=3 independent experiments. *p<0.05.

Figure 7. Effect of GPR55 disruption and pharmacological treatment on ribonucleotide reductase levels. (**a**) HPAFII cells were transfected with the indicated siRNAs or transfection reagent ("untreated") and lysed after 72h. Levels of RRM1 were assessed by Western blotting. Data from densitometry analysis are expressed as fold change of normalised results from cells transfected with siControl and are means ± s.e.m. of *n*=3 independent experiments. *p<0.05. (**b**) HPAFII cells were treated with the indicated concentrations of CBD for 24h or 72h and levels of RRM1 and RRM2 were assessed by Western blotting. Tubulin or vinculin were used as loading controls. Data from densitometry analysis are expressed as fold change of

normalised results from cells incubated with vehicle (“untreated”) and are means ± s.e.m. of *n*=3 independent experiments apart from RRM2 at 24h (*n*=4). *p<0.05, **p<0.01. (**c,d**) Representative images of PDAC specimens from KPC and KPCG mice (**c**) or KPC mice given CBD and GEM (**d**) stained with anti-RRM1 antibody. Scale bar: 50µm. Graph indicates the percentage of PDAC cells showing positive staining.

Figure 1

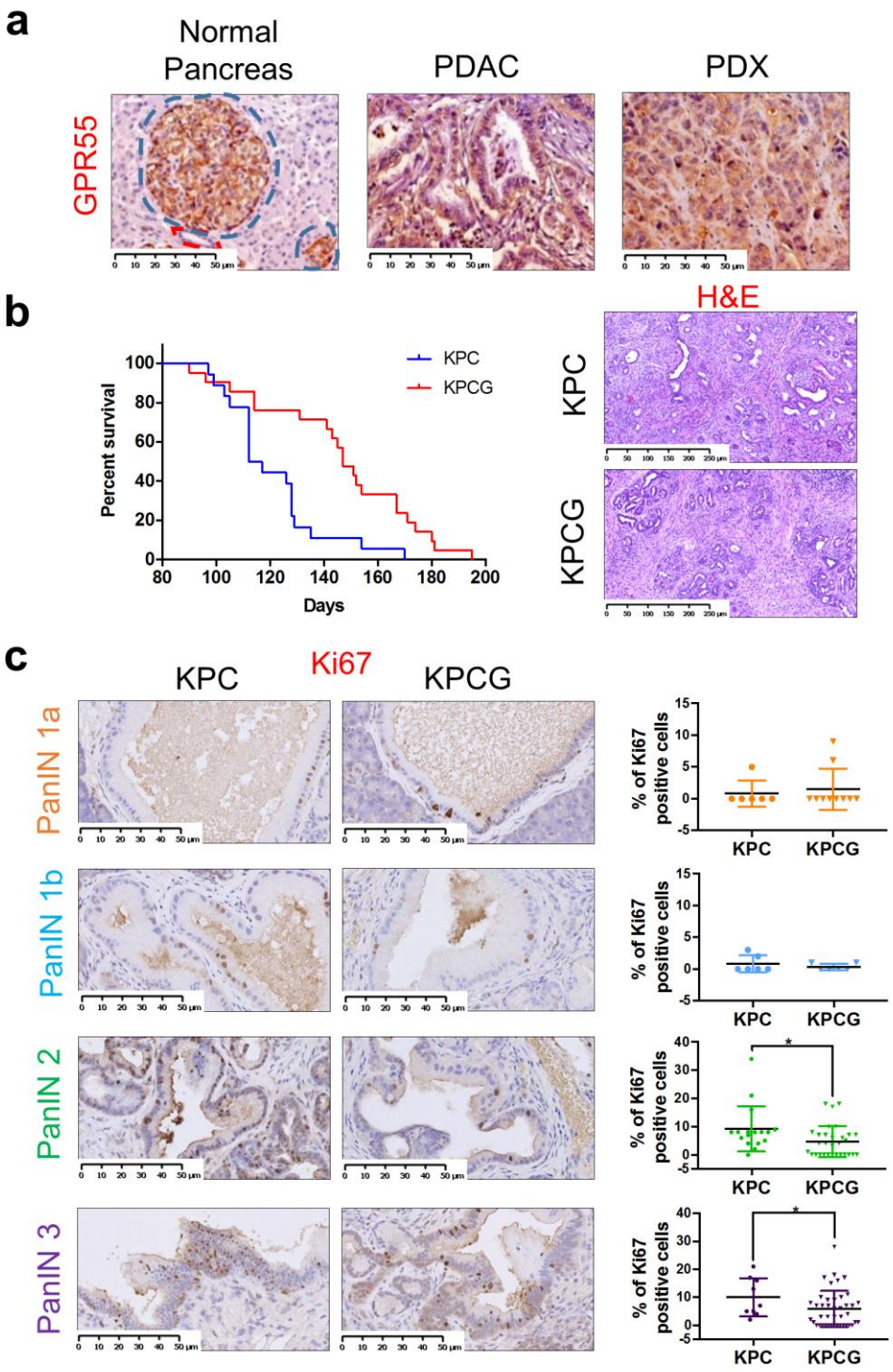
a
Normal Pancreas
PDAC
PDX
GPR55
b
H&E
KPC
KPCG
Percent survival
Days
c
KPC
Ki67
KPCG
PanIN 1a
PanIN 1b
PanIN 2
PanIN 3
% of Ki67 positive cells

Figure 2

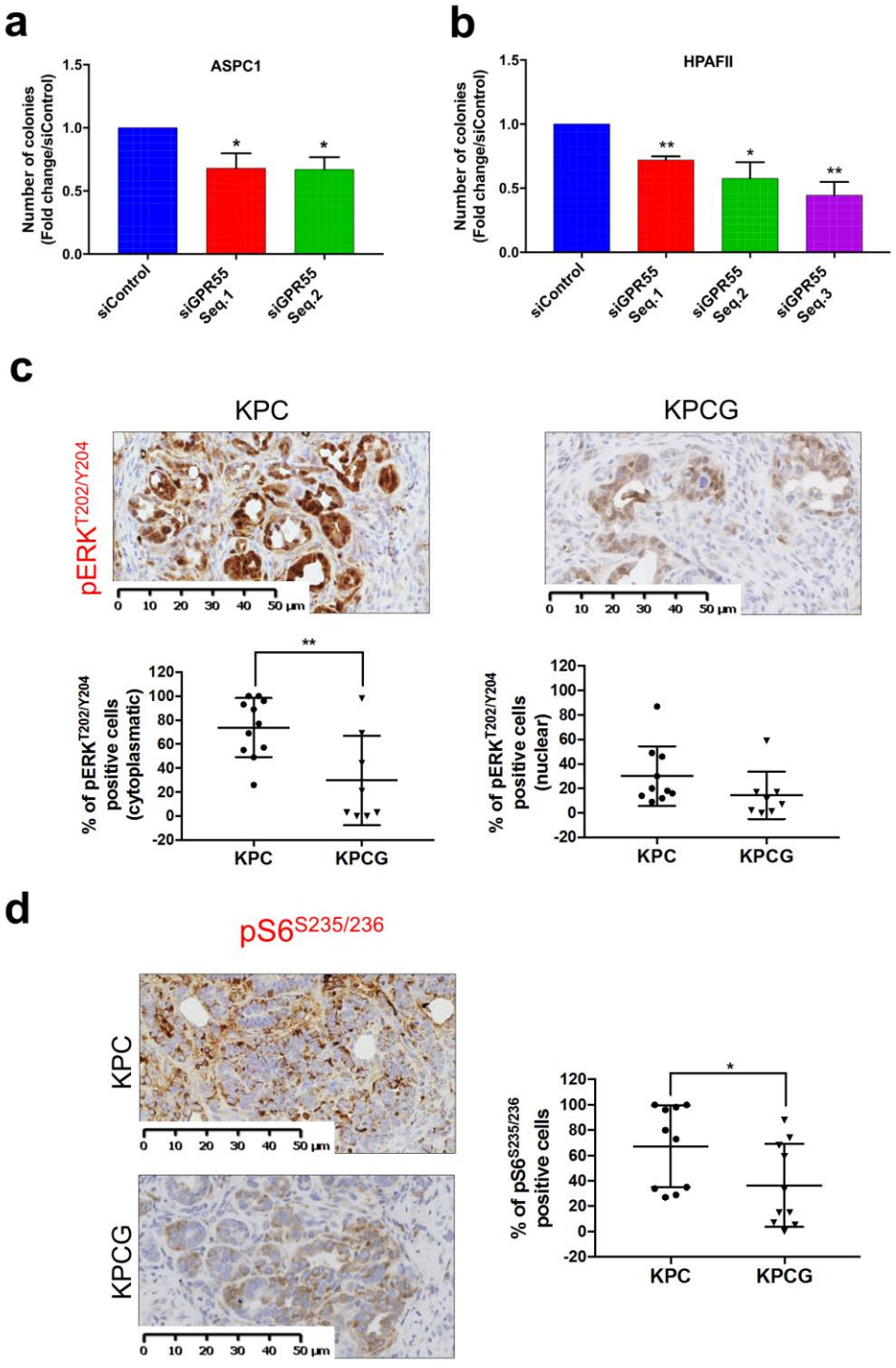
a
ASPC1
Number of colonies (Fold change/siControl)
1.5
1.0
0.5
0.0
*
*
siControl
siGPR55 Seq.1
siGPR55 Seq.2
b
HPAFII
Number of colonies (Fold change/siControl)
1.5
1.0
0.5
0.0
**
*
**
siControl
siGPR55 Seq.1
siGPR55 Seq.2
siGPR55 Seq.3
c
KPC
KPCG
pERKT202/Y204
0 10 20 30 40 50 µm
0 10 20 30 40 50 µm
**
% of pERKT202/Y204 positive cells (cytoplasmatic)
120
100
80
60
40
20
0
-20
KPC
KPCG
% of pERKT202/Y204 positive cells (nuclear)
120
100
80
60
40
20
0
-20
KPC
KPCG
d
pS6S235/236
KPC
KPCG
0 10 20 30 40 50 µm
0 10 20 30 40 50 µm
*
% of pS6S235/236 positive cells
120
100
80
60
40
20
0
-20
KPC
KPCG

Figure 3

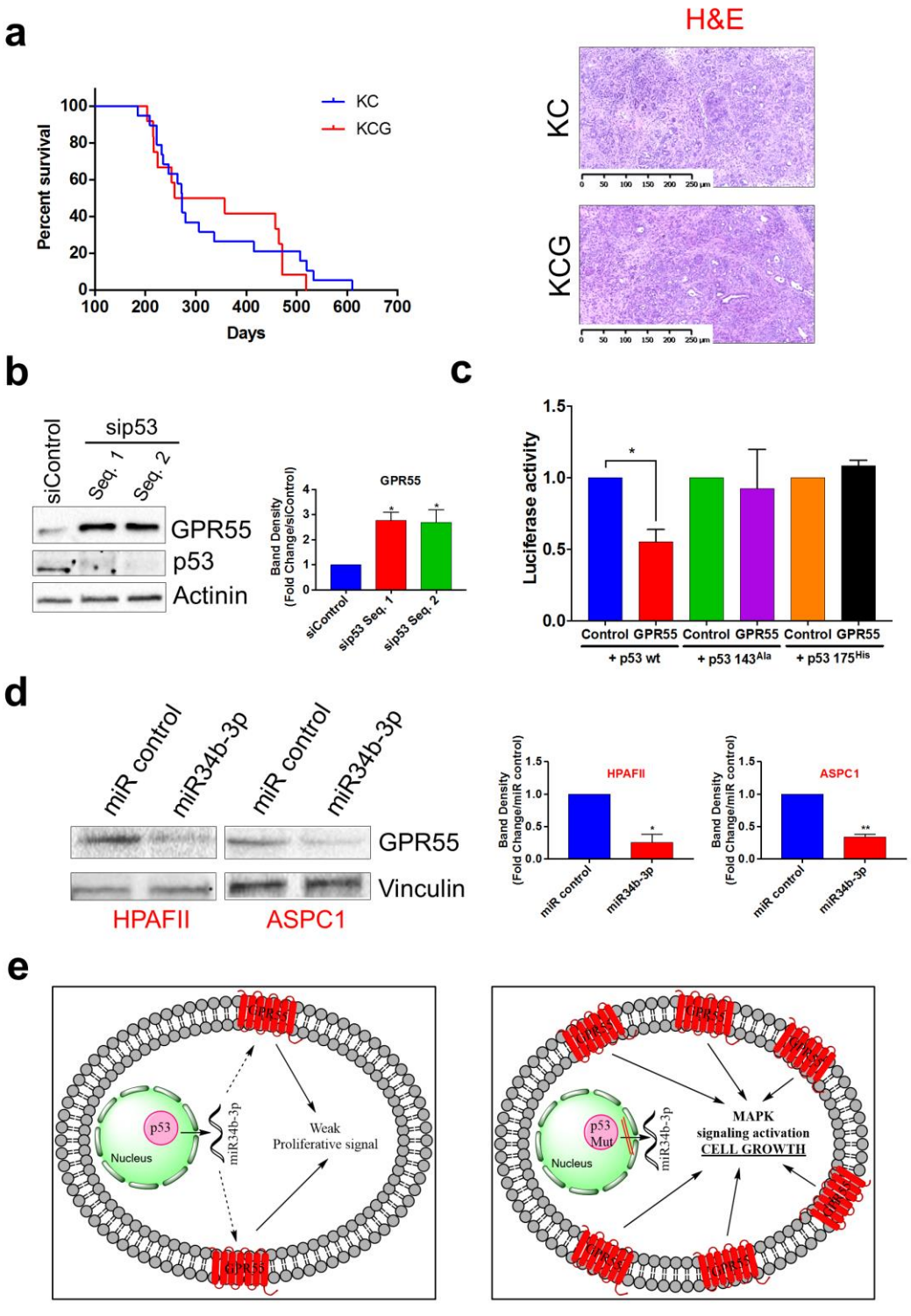
a
Percent survival
Days
KC
KCG
H&E
b
siControl
sip53
Seq. 1
Seq. 2
GPR55
p53
Actinin
Band Density (Fold Change/siControl)
siControl
sip53 Seq. 1
sip53 Seq. 2
c
Luciferase activity
Control GPR55 Control GPR55 Control GPR55
+ p53 wt
+ p53 143Ala
+ p53 175His
d
miR control
miR34b-3p
GPR55
Vinculin
HPAFII
ASPC1
Band Density (Fold Change/miR control)
e
p53
Nucleus
miR34b-3p
Weak Proliferative signal
GPR55
p53 Mut
MAPK signaling activation
CELL GROWTH

Figure 4

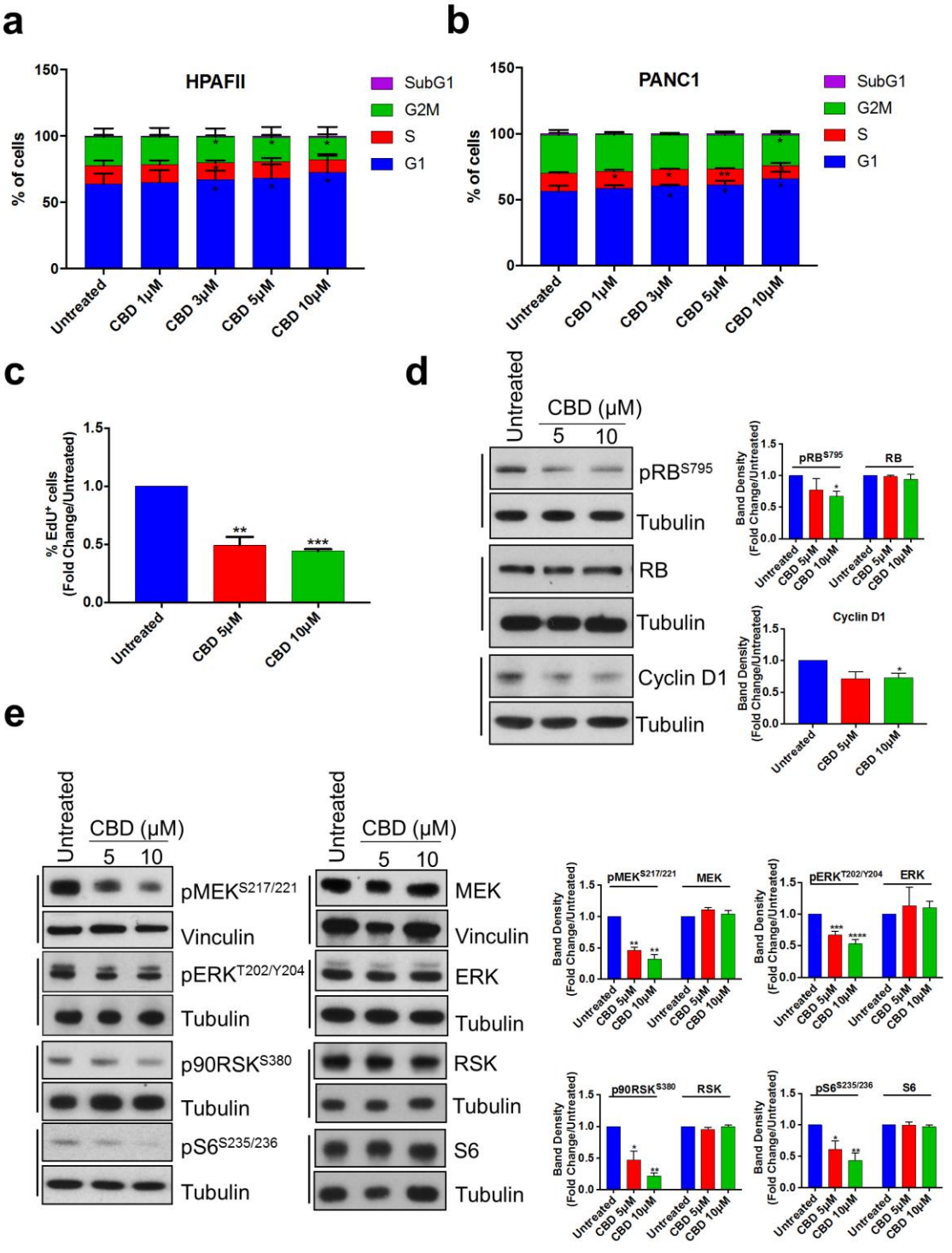
a
HPAFII
SubG1
G2M
S
G1
% of cells
Untreated
CBD 1μM
CBD 3μM
CBD 5μM
CBD 10μM
b
PANC1
c
% EdU+ cells (Fold Change/Untreated)
d
Untreated
CBD (μM)
5
10
pRBS795
Tubulin
RB
Cyclin D1
Band Density (Fold Change/Untreated)
e
pMEKS217/221
Vinculin
pERKT202/Y204
p90RSKS380
pS6S235/236
MEK
ERK
RSK
S6

Figure 5

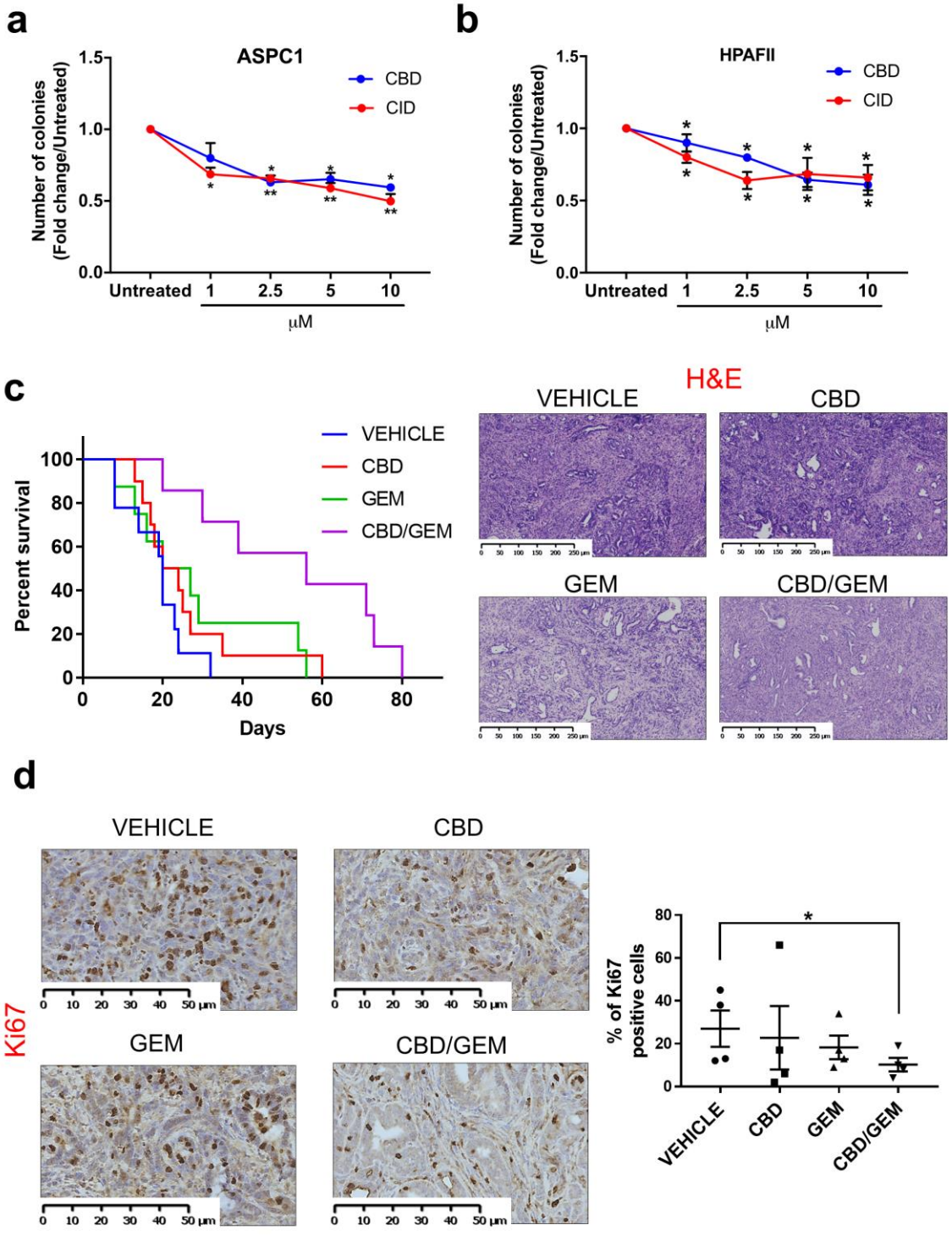
a
ASPC1
CBD
CID
Number of colonies (Fold change/Untreated)
Untreated
1
2.5
5
10
μM
b
HPAFII
CBD
CID
Number of colonies (Fold change/Untreated)
Untreated
1
2.5
5
10
μM
c
VEHICLE
CBD
GEM
CBD/GEM
Percent survival
Days
H&E
VEHICLE
CBD
GEM
CBD/GEM
d
Ki67
VEHICLE
CBD
GEM
CBD/GEM
% of Ki67 positive cells
VEHICLE
CBD
GEM
CBD/GEM

Figure 6

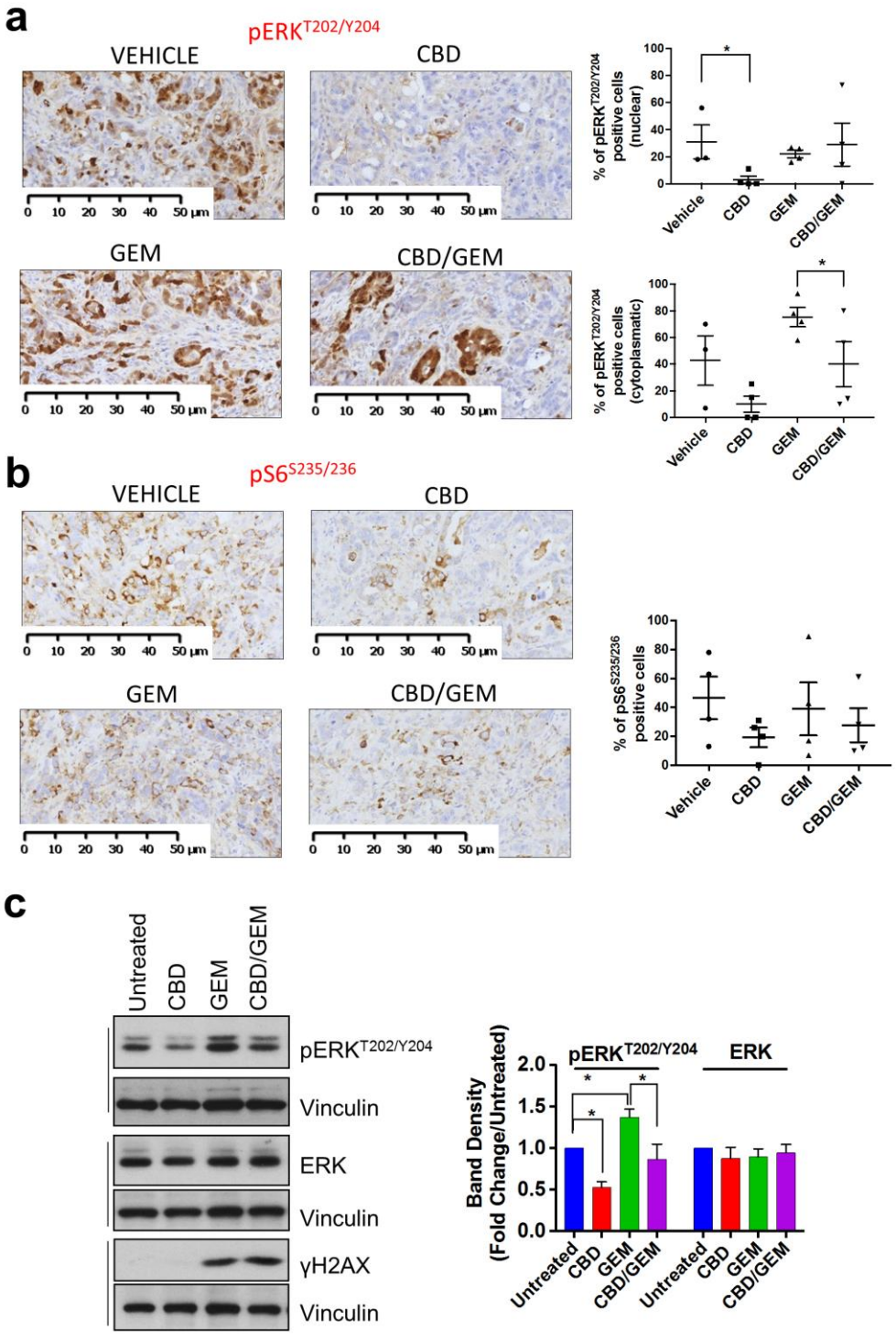
a
pERK T202/Y204
VEHICLE
CBD
GEM
CBD/GEM
0 10 20 30 40 50 µm
% of pERK T202/Y204 positive cells (nuclear)
% of pERK T202/Y204 positive cells (cytoplasmatic)
Vehicle
CBD
GEM
CBD/GEM
b
pS6 S235/236
% of pS6 S235/236 positive cells
c
Untreated
CBD
GEM
CBD/GEM
pERK T202/Y204
Vinculin
ERK
Vinculin
γH2AX
Vinculin
Band Density (Fold Change/Untreated)
pERK T202/Y204
ERK

Figure 7

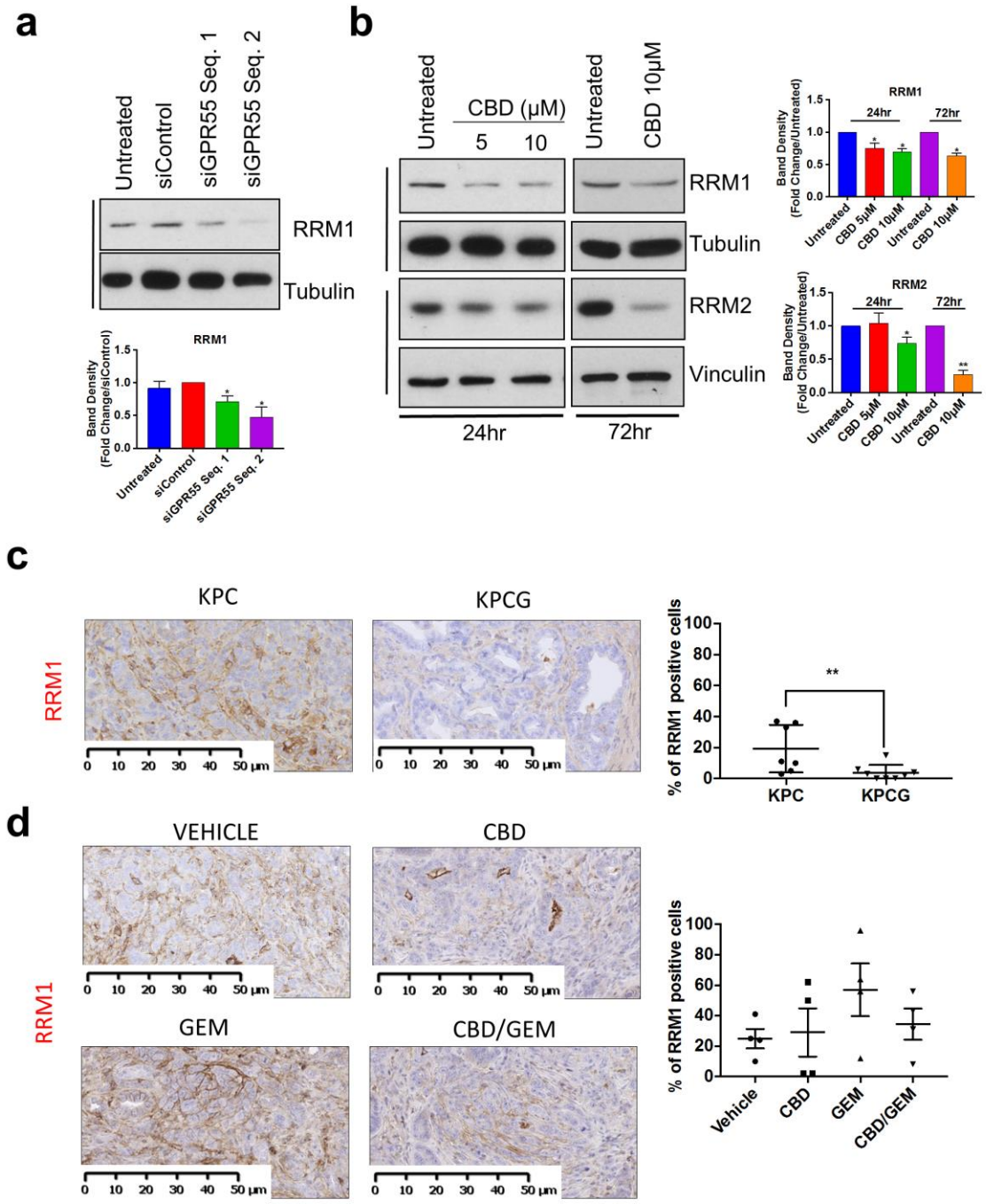
a
Untreated
siControl
siGPR55 Seq. 1
siGPR55 Seq. 2
RRM1
Tubulin
RRM1
Band Density (Fold Change/siControl)
Untreated
siControl
siGPR55 Seq. 1
siGPR55 Seq. 2
b
Untreated
CBD (μM)
5
10
Untreated
CBD 10μM
RRM1
Tubulin
RRM2
Vinculin
24hr
72hr
RRM1
Band Density (Fold Change/Untreated)
24hr
72hr
Untreated
CBD 5μM
CBD 10μM
Untreated
CBD 10μM
RRM2
Band Density (Fold Change/Untreated)
24hr
72hr
Untreated
CBD 5μM
CBD 10μM
Untreated
CBD 10μM
c
KPC
KPCG
RRM1
0 10 20 30 40 50 μm
% of RRM1 positive cells
**
KPC
KPCG
d
VEHICLE
CBD
GEM
CBD/GEM
RRM1
0 10 20 30 40 50 μm
% of RRM1 positive cells
Vehicle
CBD
GEM
CBD/GEM

GPR55 Signalling Promotes Proliferation of Pancreatic Cancer Cells and Tumour Growth in Mice, and its Inhibition Increases Effects of Gemcitabine

R Ferro,[1] A Adamska,[2] R Lattanzio,[3] I Mavrommati,[1] C E Edling,[1] S A Arifin,[1] C A Fyffe,[1] G Sala,[3] L Sacchetto,[4] G Chiorino,[4] V De Laurenzi,[2,3] M Piantelli,[3] O J Sansom,[5] T Maffucci[1] and M Falasca[1,2] .

Supplementary Information

Supplementary Materials and Methods

Cell culture and transfection

All cell lines were obtained from American Type Culture Collection (ATCC) apart from the immortalised normal pancreatic cell line HPDE, kindly provided by Prof Hemant Kocher (Queen Mary University of London). Cell lines were authenticated and routinely tested for mycoplasma contamination. All cell lines (apart from HPDE) were cultured in DMEM supplemented with 10% (v/v) fetal bovine serum (FBS), 1X penicillin/streptomycin and glutamine, and 1% (v/v) sodium pyruvate. HPDE cells were cultured in keratinocyte serum-free medium supplemented with epidermal growth factor and bovine pituitary extract. Cells were maintained under standard cell culture conditions (37°C, 20% O_2, 5% CO_2). siRNAs were transfected using Oligofectamine™ or Lipofectamine® RNAiMAX, according to the manufacturer's instructions.

Cell growth assays

For cell counting, cells were seeded in 12 well plates and grown in cell culture medium supplemented with 10% FBS for the indicated times. When necessary, cells were treated with the GPR55 antagonists CBD or CID16020046 (Tocris Bioscience). The number of cells was assessed after 72 h by cell counting. For anchorage-independent growth, 1.2% agarose gel was melted and then placed in a water bath at 55°C. DMEM medium was supplemented with 20% (v/v) FBS, 2X penicillin/streptomycin and glutamine and 2% (v/v) sodium pyruvate (2X DMEM), and kept at 37°C. A mix of 1.2% melted agarose gel and 2X DMEM was used to generate 2ml 0.6% agarose thick base layer. The mix was poured into one well of a 6-well plate and left to solidify. Where indicated, cells were transfected for 24 h. Cells were washed, detached, counted and a suspension of 20,000 cells was prepared in 1.5ml of 2X DMEM. Then 0.75ml of 1.2% agarose gel and 0.75ml of 2X DMEM was mixed to form a 0.3% agarose gel. The mix was poured on top of the solidified 0.6% agarose gel. 2ml of DMEM was added on top and cells were left to grow at 37°C in a 5% CO_2 atmosphere. Colonies were fixed with

4% paraformaldehyde or methanol/acetic acid in PBS 3-4 weeks after plating, stained with Crystal Violet (0.05%) and counted under the microscope or using the ChemiDoc XRS+ System (Bio-Rad).

Cell cycle analysis

Cells were seeded in a 6 well plate (200,000 cells/well) and transfected with the indicated siRNAs or treated with CBD. At indicated times, cells were washed once with PBS, detached and collected in 1.5ml microfuge tubes and centrifuged at 1,200 rpm for 5 min. Pelleted cells were then fixed in ice-cold 70% ethanol by adding one drop at a time on a vortex and left at 4°C from 60 min to a week. Cells were then washed and centrifuged at 1,200 rpm for 5 min and re-suspended in 200µl Vindellövs Propidium Iodide (PI) solution (50µg/ml PI, Ribonuclease I 100µg/ml) before being analysed by FACS, collecting 50,000 events per sample.

EdU assay. To assess EdU incorporation, cells were treated with 5µM or 10µM of CBD for 70 h and then treated with 10µM EdU for 2 h. Cells were fixed in 70% ethanol for 1 h and then treated according to the manufacturer's instructions (Thermo Fisher Scientific). Cells were washed and centrifuged at 1,200 rpm for 5 min and resuspended in 500µl Vindellövs PI solution before being analysed by flow cytometry, collecting 50,000 events per sample using FACS Diva software.

Apoptosis assays

For the Annexin V assay, cells were plated in 6 well plates (200,000 cells/well) and transfected with the indicated siRNAs. At 48 h post transfection, cells were collected (including the supernatant) and pelleted. The pellet was resuspended in 400µl 1X Annexin V Binding Buffer and 2µl of Annexin V-FITC and incubated in the dark for 15 min at room temperature. Then, 4µl PI was added and the samples were analysed using FACS Diva software, collecting 20,000 events per sample. A control of unstained cells was incubated with 1X Annexin V

Binding Buffer alone and Annexin V-FITC or PI in order to set the quadrants. Caspase 3 activity was measured by using an EnzCheck® Caspase 3 Assay Kit #2 (Cat. No E-13184, Molecular Probes®, Life Technologies) according to manufacturer's instructions. Cells were plated in 6 well plates (200,000 cells/well) and transfected with indicated siRNAs. At 48 h post transfection, cells were washed once with PBS and pelleted. The pellets were then resuspended in 100µl 1X cell lysis buffer solution and kept on ice for 30 min. Cell lysates were then centrifuged at 5,000 rpm for 5 min and the supernatant was transferred to a new 1.5ml microfuge tube. 1X cell lysis buffer was used as a control to determine background fluorescence of the substrate. 50µl of 2X substrate working solution was added in each sample and control and 100µl were transferred in a 96 well plate and incubated for 75 min at room temperature. Fluorescence was then measured using a spectrophotometer (Synergy HT) at excitation/emission 496/520nm. The protein concentration of each sample was determined using the Bradford or BCA protein assay. Fluorescence results were then normalised according to the protein concentration of each sample.

RT-qPCR analysis

RNA was extracted from cells or murine tissues using the GeneJET RNA Purification Kit (Thermo Fisher Scientific) according to the manufacturer's instructions. The complementary DNA (cDNA) synthesis was performed on ice using Maxima Reverse Transcriptase (Thermo Fisher Scientific) according to the manufacturer's instructions. RT-qPCR was performed using 2X Maxima SYBR green/Fluorescein (Fermentas) qPCR mix and the ABI 7500 RT-QPCR. QARS, GAPDH or RPS14 cDNA were also amplified as housekeeping gene controls. All experiments were performed in triplicate. Quantification of the relative changes in gene expression was calculated using the relative ddCT analysis mode of the ABI 7500 Real-Time PCR system software. GAPDH forward and reverse primers 5'-AGGGCTGCTTTTAACTCTGGT-3', 5'-CCCCACTTGATTTTGGAGGGA-3'; GPR55 forward and reverse primers 5'-GTTTCCATGGGAAAGTGGAA-3', 5'-GGAAGGAGACCACGAAGACA-3'; QARS forward and reverse primers 5'-

CAGGGGTCTGGCTTATGTGT-3' 5'-CTCTGAAAACTTGCCCTTGC-3'. RRM1 forward and reverse primers 5'-ACTAAGCACCCTGACTATGCTATCC-3' 5'-CTTCCTCACATCACTGAACACTTT-3' RPS14 forward and reverse primers 5'-GACCAAGACCCCTGGACCT-3' 5'-CCCCTTTTCTTCGAGTGCTA-3'

Immunoblotting

Cells were washed and lysed either in 2% SDS or in ice-cold lysis buffer [50 mM Tris, pH 7.5, 150mM NaCl, 1% Triton X-100, 2mM EDTA, 2mM EGTA, 1µl/ml Protease inhibitor cocktail (Sigma Aldrich), 1µl/ml Phosphatase inhibitor cocktail A (Sigma Aldrich) and 1µl/ml Phosphatase inhibitor cocktail B (Sigma Aldrich)]. Samples were separated by SDS-PAGE and transferred to nitrocellulose membranes. Membranes were then incubated in PBS supplemented with 0.05% (v/v) Tween 20 (PBS-T) containing 5% skim milk powder for 1 h at room temperature, followed by overnight incubation with primary antibodies at 4°C. After washing with PBS-T, membranes were incubated with secondary antibodies for 1 h at room temperature, washed with PBS-T and exposed to ECL reagent. Anti-p53 (1:1000, Cell Signaling Technology, product code 2527); anti-Tubulin (1:10000, Sigma-Aldrich, product code T9026); anti-pERK$^{T202/Y204}$ (1:2000, Cell Signaling Technology, product code 4370); anti-pS6$^{S235/236}$ (1:1000, Cell Signaling Technology, product code 4858); anti-pMEK$^{S217/221}$ (1:1000, Cell Signaling Technology, product code 9154); anti-p90RSK^{S380} (1:1000, Cell Signaling Technology, product code 11989); anti-RRM1 (1:1000, Santa Cruz Biotechnology, product code sc-11733); anti-RRM2 (1:1000, Santa Cruz Biotechnology, product code sc-10846); anti-Vinculin (1:1000, Cell Signaling Technology, product code 4650); anti cyclin D1 (1:1000, Cell Signaling Technology, product code 2978); anti ERK2 (1:1000, Santa Cruz Biotechnology, product code sc-154); anti RSK1/RSK2/RSK3 (1:1000, Cell Signaling Technology, product code 9355); anti MEK1/2 (1:1000, Cell Signaling Technology, product code 4694); anti S6 (1:1000, Cell Signaling Technology, product code 2317); anti actinin (1:1000, Cell Signaling Technology, product code 3134). For GPR55 staining, membranes were incubated in TBS containing 0.05% Tween (TBS-T) supplemented with 3% BSA for 1 h before overnight

incubation with anti-GPR55 (1:80,000, Cayman Chemical, product code 10224). Densitometry analysis was performed using Image J. In all graphs, specific band densities were normalised to the corresponding loading control.

microRNA (miR) analysis

To assess miR levels, cells were washed twice with PBS and lysed using Qiazol Lysis Reagent (Qiagen). Total RNA was extracted using miRNAs Mini Kit (Qiagen), and cDNA synthesised using TaqMan® MicroRNA Reverse Transcription kit (Life Technologies) according to the manufacturer's instructions. PCR was performed according to the manufacturer's instructions (TaqMan® MicroRNA Assays Protocol, Life Technologies). Analysis of miR expression was performed using the cycle threshold (Ct) and RNU48 as endogenous control. Levels of miRs were obtained using the $\Delta\Delta$Ct method and expressed as $2(-\Delta\Delta Ct)$ values.

Luciferase assay

Plasmids encoding the luciferase gene either under the control of the 3'-UTR of the GPR55 (defined as "GPR55" in Figure 3c) or without a regulatory region (defined as "Control" in Figure 3c) were used. Both plasmids were purchased from ABM®. ASPC1 cells were plated in a 24 well plate and transiently co-transfected with each 3'-UTR plasmid in combination with an empty vector (pcDNA) or a plasmid encoding either wild type (wt) or p53 mutants (p53 143^{Ala}, p53 175^{His}). This led to two groups of transfected cells: *a)* cells co-transfected with "Control" and either pcDNA or p53 wt or p53 mutants; *b)* cells co-transfected with "GPR55" and either pcDNA or p53 wt or p53 mutants. Assays were performed by using the Luciferase assay system (Promega, cat number E1500) according to the manufacturer's instructions. For each group of transfections (*a* & *b*), results were expressed as fold change of normalised luciferase activity in cells co-transfected with pcDNA. To obtain final results, values for group *b* were expressed as fold change of corresponding values in group *a*. Plasmids encoding p53 carrying gain-of-function mutations at positions 143^{Ala} or 175^{His} were kindly provided by Dr Massimo Broggini (IRCCS, Istituto di Ricerche Farmacologiche Mario Negri, Milan, Italy).

Human phospho-kinase array

HPAFII cells were treated with 10µM CBD or vehicle alone in DMEM containing 10% FBS for 24h before being lysed. Analysis of the phosphorylation status of several kinases was performed using Proteome Profiler Human Phospho-Kinase Array Kit (Cat. No. ARY003B, R&D Systems, Abingdon, UK) according to the manufacturer's instructions. Densitometry analysis was performed using Image J software according to the manufacturer's instructions.

Supplementary Figure legends

Supplementary Figure 1. GPR55 expression in PDAC. (**a**) Representative Western blot of GPR55 protein expression in a panel of PDAC cell lines. Tubulin was used as loading control. All cell lines in figure harbour *TP53* mutations. (**b**) Representative IHC images of GPR55 protein expression in pancreas from Pdx1-Cre$^{+/+}$ mice as well as images of non-neoplastic pancreas and PDAC tissues from KPC mice. Images of non-neoplastic pancreas and PDAC tissues from KPCG mice incubated with the anti GPR55 antibody are also shown. Blue dotted lines indicate Islet of Langerhans, red dotted lines indicate normal pancreatic duct. Scale bar: 50μm.

Supplementary Figure 2. Effect of GPR55 downregulation on PDAC cell growth. ASPC1 (**a,b**), HPAFII (**c,d**), and PANC1 (**e,f**) were transfected with a non-targeting siRNA (siControl), siRNAs specifically targeting GPR55 or transfection reagent alone ("untreated"). In **a**, **c** and **e** the number of cells was assessed at 72 h post transfection by manual counting as described in the Materials and Methods section. Data are expressed as fold change of untreated cells and are means ± s.e.m. of *n*=3 independent experiments performed in duplicate. *p<0.05, **p<0.01, ***p<0.001 vs untreated cells. (**b,d,f**) Representative RT-qPCR of GPR55 mRNA levels in cells transfected with the indicated siRNAs at 72 h post transfection. QARS was used as a housekeeping gene. Data are expressed as fold change of cells transfected with siControl and are means ± s.e.m. of *n*=3 independent experiments performed in duplicate. *p<0.05, **p<0.01, ***p<0.001 vs cells transfected with siControl.

Supplementary Figure 3. GPR55 regulation of PDAC cell cycle and MAPK/ERK signalling pathways. (**a,b**) Effect of GPR55 downregulation on HPAFII (**a**) and PANC1 (**b**) cell cycle. Cell cycle analysis was performed by FACS at 48 h after transfection. Cells were grown in DMEM containing 10% FBS. Results are expressed as percentage of cells in each phase of the cycle and are means ± s.e.m. of *n*=3 independent experiments. *p<0.05, **p<0.01, ***p<0.001 vs

cells transfected with siControl. (**c**) Effect of GPR55 downregulation on Cyclin D1, Cyclin D2, and Cyclin B1 mRNA levels assessed by RT-qPCR. GAPDH was used as a housekeeping gene. Results are expressed as fold change of cells transfected with siControl and are means ± s.e.m. of *n*=3 independent experiments. *p<0.05; **p<0.01. (**d**) ASPC1 cells were transfected with the indicated siRNAs or transfection reagent alone ("untreated") and the activity of caspase 3 was assessed at 48 h post transfection. Data are expressed as fold change of caspase 3 activation in untreated cells and are means ± s.e.m. of *n*=2 independent experiments. (**e**) HPAFII cells were transfected with the indicated siRNAs or transfection reagent alone ("untreated") and analysed at 48 h post transfection by Annexin V/FACS analysis as described in the Materials and Methods section. Results indicate the percentage of apoptotic cells (early and late apoptotic cells) and are means ± s.e.m. of *n*=2 independent experiments. (**f**) Effect of GPR55 downregulation on $pERK^{T202/Y204}$ and $pS6^{S235/236}$ and total ERK and S6 levels, assessed by Western blotting analysis. Tubulin and vinculin were used as loading controls. Data from densitometry analysis are expressed as fold change of normalised results from cells transfected with siControl and are means ± s.e.m. of *n*=3 independent experiments. *p<0.05, **p<0.01.

Supplementary Figure 4. p53 regulates GPR55 through miR regulation. (**a**) Western blotting analysis of GPR55 protein expression in PDAC murine cell lines derived from the indicated mouse models. Tubulin was used as loading control. Data from densitometry analysis are expressed as fold change of normalised levels of GPR55 in PZR1 cells and are means ± s.e.m. of *n*=3 independent experiments. *p<0.05, **p<0.01. (**b**) ASPC1 cells were transfected with a plasmid encoding wild type p53 or corresponding empty vector (pcDNA). Levels of GPR55 were assessed by Western blotting analysis. Tubulin was used as loading control. Data from densitometry analysis are expressed as fold change of normalised levels of GPR55 in cells transfected with pcDNA and are means ± s.e.m. of *n*=3 independent experiments. *p<0.05. (**c**) HEK293T cells, expressing wild type p53, were transfected with two siRNAs specifically targeting p53 and a non-targeting siRNA (siControl). Cells were lysed after 48 h

and levels of GPR55 and p53 were assessed by Western blotting analysis. Actinin was used as loading control. Representative blot and results from densitometry analysis are shown. Data are means ± s.e.m. of *n*=3 independent experiments and are expressed as fold change of GPR55 levels normalised to loading control in cells transfected with siControl. *p<0.05, **p<0.01. (**d**) ASPC1 cells were transfected with plasmids expressing the luciferase gene under the control of the 3'-UTR of GPR55 ("GPR55") or the luciferase gene without regulatory regions ("Control") in combination with pcDNA or plasmids encoding wild type or the indicated mutants p53. Expression levels of the exogenous proteins were assessed by Western blotting analysis. Tubulin was used as loading control. (**e**) In silico analysis of 3'-UTR GPR55 binding site showing matching sequences with hsa-miR34b-3p. (**f**) Levels of miR34b-3p in HPDE, ASPC1 and HPAFII cells assessed by RT-qPCR. *n*=2. (**g**) ASPC1 cells were transfected with a plasmid encoding wild type p53 or empty vector. At the indicated times, levels of miR34b-3p were assessed by RT-qPCR.

Supplementary Figure 5. Effect of pharmacological inhibition of GPR55 on PDAC cell growth. ASPC1 (**a**), HPAFII (**b**), BXPC3 (**c**) and PANC1 (**d**) cells were treated with the indicated concentrations of drugs in DMEM containing 10% FBS. The number of viable cells was assessed after 72 h by manual counting. Control cells were incubated with the corresponding amount of vehicle ("untreated"). Data are expressed as fold change of control cells and are means ± s.e.m. of *n*=3 independent experiments performed in duplicate. *p<0.05, ** p<0.01, *** p<0.001 vs control cells.

Supplementary Figure 6. Effect of CBD on a panel of kinases and related proteins. Results from densitometry analysis of the phospho-kinase array assay performed in HPAFII treated with 10μM CBD or incubated with vehicle alone (untreated). For each protein data show values from CBD-treated sample expressed as fold change compared to the corresponding value from the untreated sample.

Supplementary Figure 7. Effect of combination of pharmacological inhibition of GPR55 and GEM on PDAC cell growth. HPAFII (**a**) and PANC1 (**b**) cells were treated with the indicated concentrations of drugs alone or in combination in DMEM containing 10% FBS and the number of cells was assessed after 72 h. Control cells were incubated with the corresponding amount of vehicle ("untreated"). Data are expressed as fold change of control cells and are means ± s.e.m. of *n*=3 (**a**) and *n*=4 (**b**) independent experiments performed in duplicate. *p<0.05, **p<0.01, ***p<0.001, ****p<0.0001.

Supplementary Figure 8. Effect of GPR55 inhibition and ablation on RRM1 mRNA levels. (**a**) HPAFII cells were treated with 10μM CBD for 48h or incubated with vehicle, DMSO, alone (untreated). Effect on RRM1 mRNA levels was assessed by RT-qPCR. GAPDH was used as housekeeping gene. Results are expressed as fold change of levels in untreated cells and are means ± s.e.m. of *n*=3 independent experiments. **p<0.01. (**b**) RNA was extracted from pancreata from KPC (*n*=5) and KPCG (*n*=6) mice and the levels of RRM1 mRNA were assessed by RT-qPCR. RPS14 was used as housekeeping gene. **p<0.01.

Supplementary Table 1. miR34 family members that are predicted to target GPR55.

Supplementary Table 2. Values of combination index (CI) and dose reduction index (DRI) for the indicated combinations as assessed by CompuSyn software. CI<1, CI=1, CI>1 indicate synergism, additivity and antagonism respectively.

Supplementary Table 3. Representative images of IHC antibody optimisation (positive and negative staining).

Supplementary Figure 1

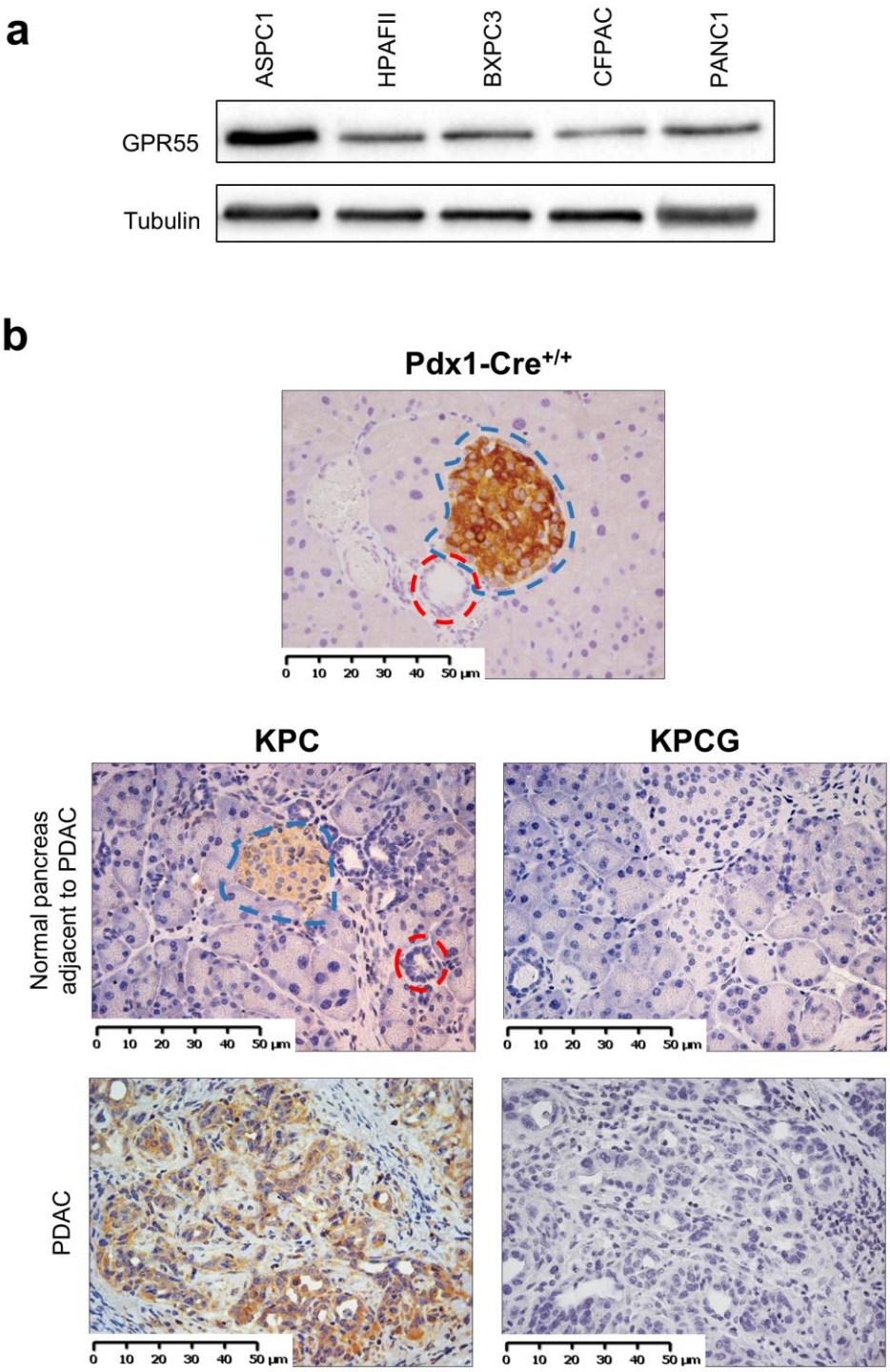

Supplementary Figure 2

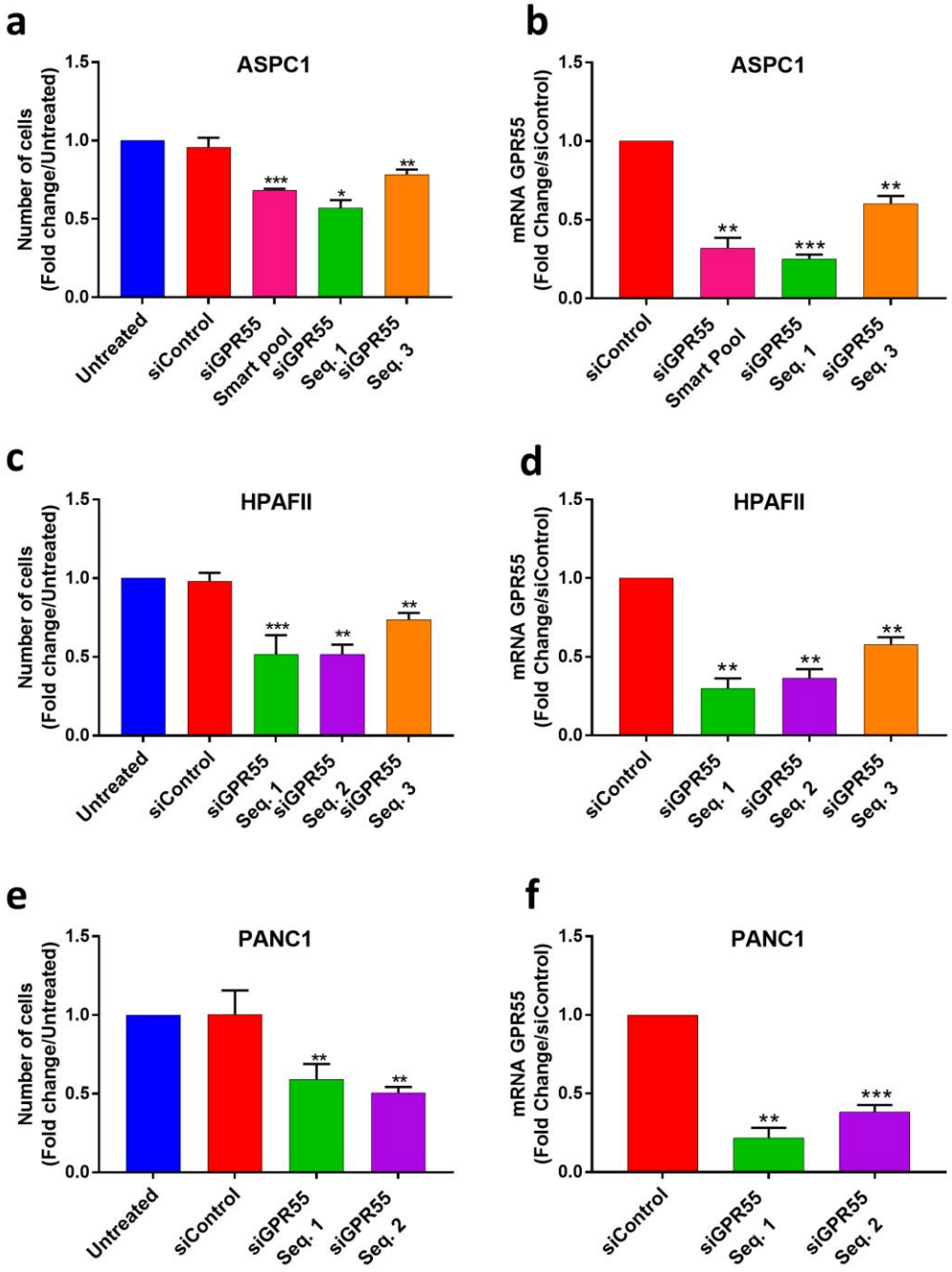

Supplementary Figure 3

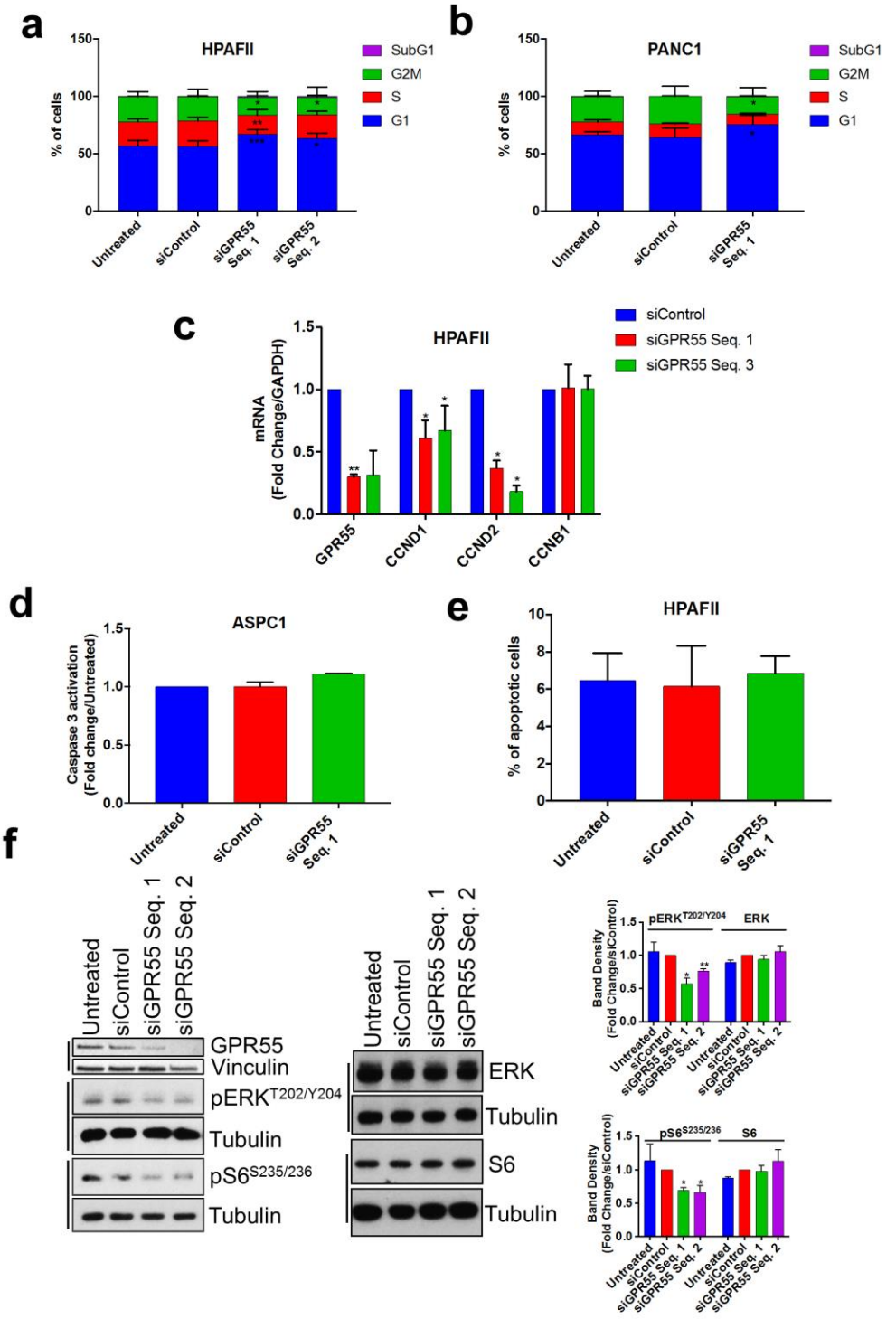

Supplementary Figure 4

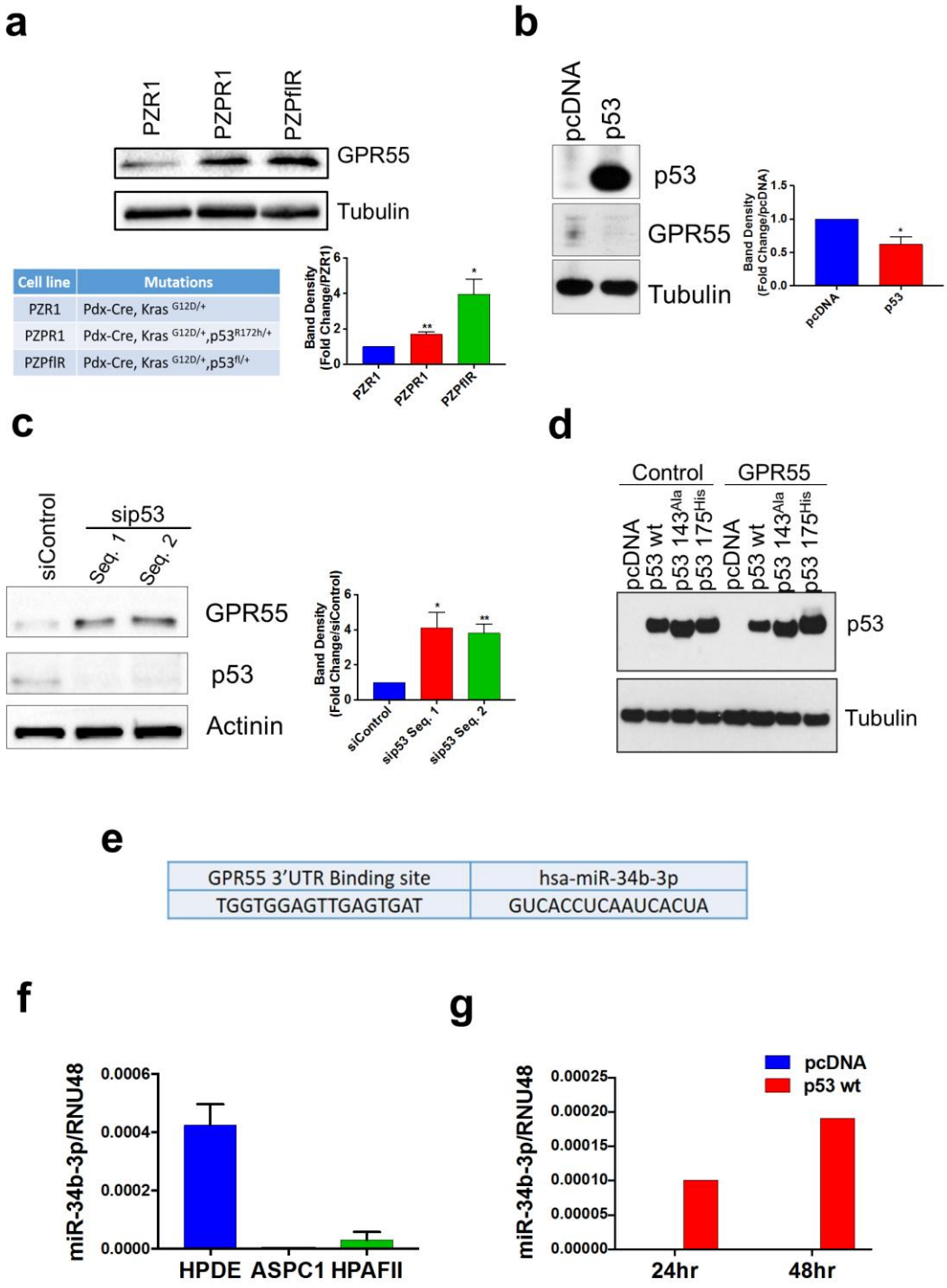

Supplementary Figure 5

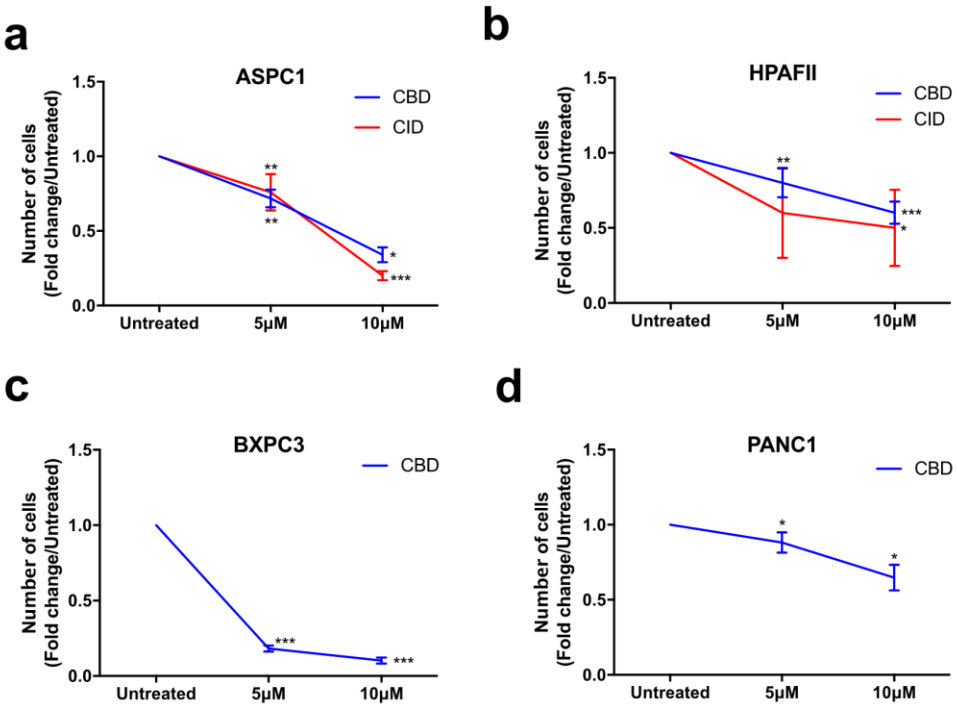

Supplementary Figure 6

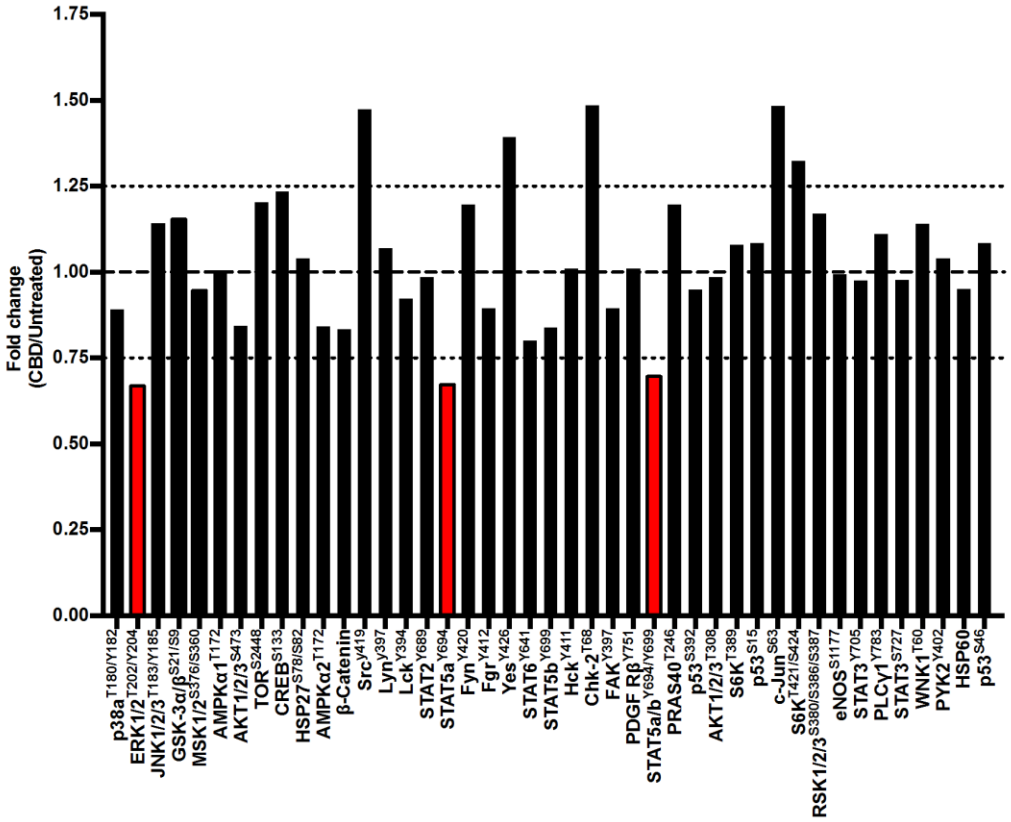

Supplementary Figure 7

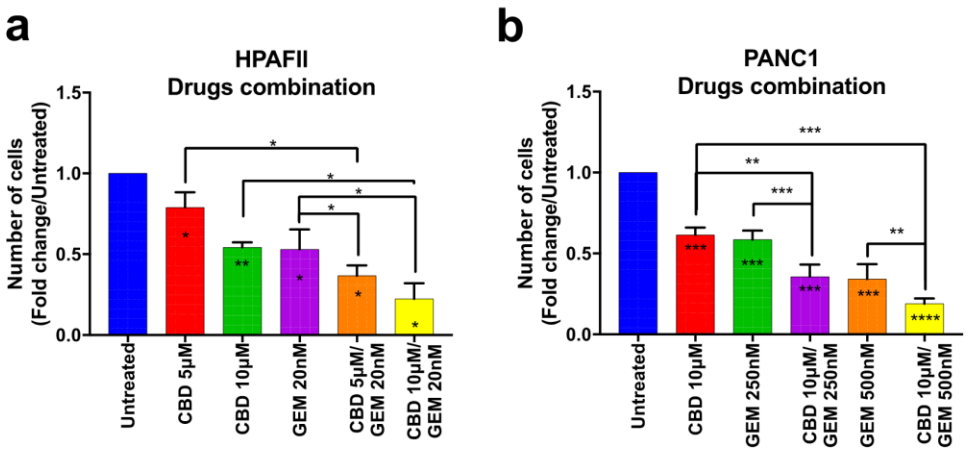

Supplementary Figure 8

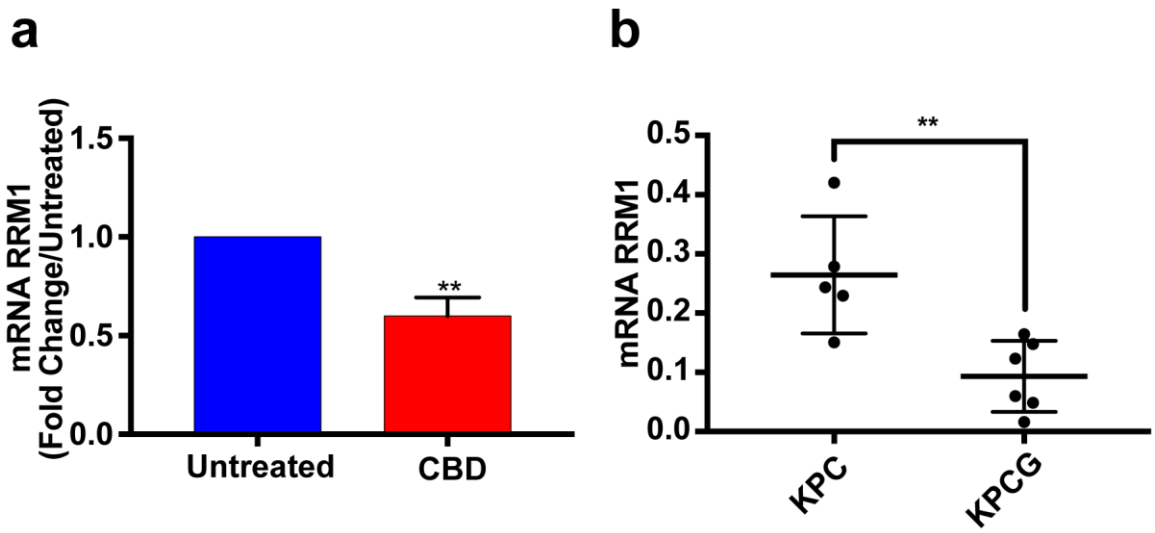

Supplementary Table 1

miRNA	MIMATid	miRWalk	microcosm	Microt4	miRanda	mirbridge	miRDB	miRMap	PITA	RNA22	RNAhybrid	Targetscan	SUM
hsa-miR-34c-5p	MIMAT 0000686	0	0	1	1	0	0	1	1	1	1	1	7
hsa-miR-34a-5p	MIMAT 0000255	0	0	0	1	0	0	1	1	1	1	1	6
hsa-miR-34b-5p	MIMAT 0000685	0	0	1	0	0	0	1	0	1	1	0	4
hsa-miR-34c-3p	MIMAT 0004677	0	0	0	0	0	0	1	1	1	1	0	4
hsa-miR-34a-5p	MIMAT 0000255	0	0	0	1	0	0	1	0	0	1	1	4
hsa-miR-34c-5p	MIMAT 0000686	0	0	0	1	0	0	1	0	0	1	1	4
hsa-miR-34b-3p	MIMAT 0004676	1	1	0	0	0	0	0	0	0	1	0	3
hsa-miR-34a-3p	MIMAT 0004557	0	0	1	0	0	0	1	0	0	1	0	3
hsa-miR-34a-3p	MIMAT 0004557	0	0	0	0	0	0	1	0	0	1	0	2
hsa-miR-34b-5p	MIMAT 0000685	0	0	0	0	0	0	1	0	0	1	0	2
hsa-miR-34c-3p	MIMAT 0004677	0	0	0	0	0	0	1	0	0	1	0	2

Supplementary Table 2

	CBD (μM)	GEM (nM)	Combination CI	Combination DRI CBD	Combination DRI GEM
HPAFII					
	5	20	0.70367	5.71002	1.89202
	10	20	0.47943	5.21714	3.47520
PANC1					
	10	250	0.87078	2.01530	2.66969
	10	500	0.65784	3.54951	2.65876

Supplementary Table 3

	IHCs Positive control	IHCs Negative control	Tissue
GPR55	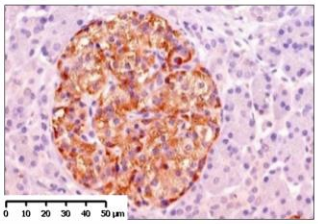	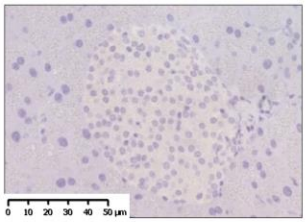	Pancreas (Islet of Langerhans)
Ki67	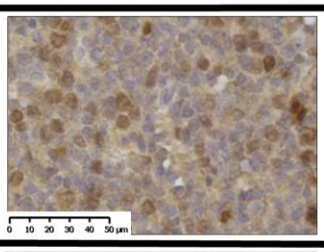	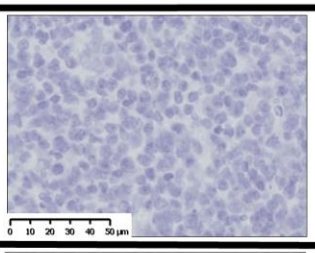	Tonsil
pERK T202/Y204	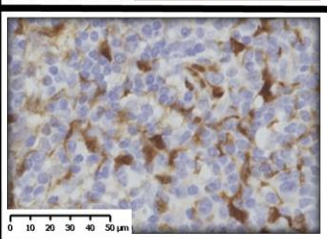	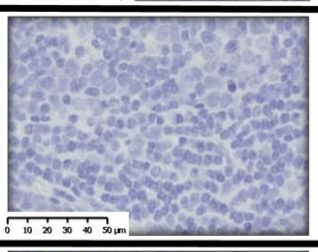	Tonsil
pS6 S235/236	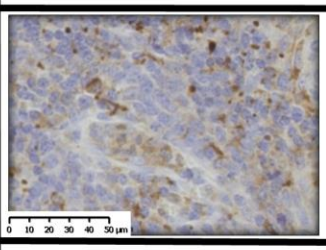	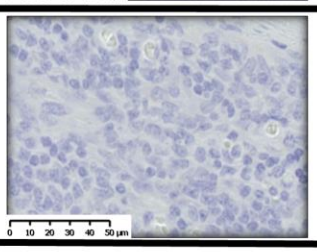	Tonsil
RRM1	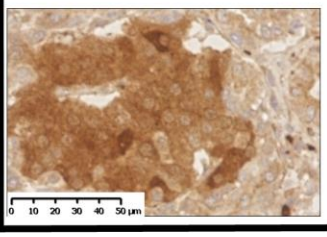	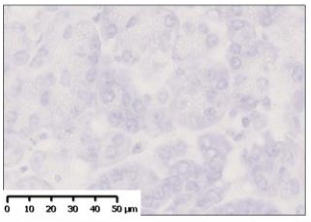	Brain